# Mechanisms of air-sea $CO_2$ exchange in the central Baltic Sea

**Yuanxu Dong[1,2], Christa A. Marandino[1], Ryo Dobashi[3], David T. Ho[3], Gregor Rehder[4], Henry C. Bittig[4], Josefine Karnatz[1], Bita Sabbaghzadeh[4], Helen Czerski[5], Anja Engel[1]**

[1]Marine Biogeochemistry Research Division, GEOMAR Helmholtz Centre for Ocean Research Kiel, Kiel, Germany

[2]Institute of Environmental Physics, Heidelberg University, Heidelberg, Germany

[3]Department of Oceanography, University of Hawai'i at Mānoa, Honolulu, Hawaii, USA

[4]Leibniz Institute for Baltic Sea Research Warnemünde, Rostock, Germany

[5]Department of Mechanical Engineering, University College London, London, UK

*Correspondence to:* Yuanxu Dong (ydong@geomar.de)

**Abstract** Air-sea gas exchange regulates the cycling of climate-relevant gases such as carbon dioxide ($CO_2$), yet significant uncertainties remain in its quantification. The gas transfer velocity ($K$), a key parameter for estimating $CO_2$ flux, is usually expressed as a function of wind speed ($U_{10N}$). This approach overlooks the role of fetch and surfactants, which can substantially affect $K$. However, no field study has systematically quantified their combined effects under fetch-limited and surfactant-abundant ocean conditions. To fill this research gap, we conducted air-sea gas exchange studies during a cruise in the central Baltic Sea, a system with high surfactant levels and a short fetch. We report independent determinations of $K$ using eddy covariance (EC) and dual-tracer ($^3He/SF_6$) techniques, together with direct measurements of natural surfactants and modelled wave parameters. Both methods yield consistent results; however, EC-based $CO_2$ transfer velocities are, on average, 33% lower than those reported in previous EC studies in the open ocean. Sea-state-dependent parameterisations indicate that limited fetch reduces $K$ by 8%, while elevated surfactant concentrations may have contributed to the additional 25% reduction. We developed an updated parameterisation that includes wind stress, sea state, and surfactants. When applied to climatological forcing, it yields a 40% stronger seasonal cycle (greater oceanic uptake during summer and enhanced outgassing during winter) of $CO_2$ flux in the Baltic Sea than obtained with the conventional $U_{10N}$-based parameterisation. These findings highlight the need to move beyond

$U_{10N}$ in parameterising $K$ and estimating regional fluxes, especially when evaluating the potential of marine carbon dioxide removal (mCDR) in coastal seas.

**Short summary** Air-sea gas exchange regulates the Earth's climate. However, the description of the kinetic exchange process only uses wind speed, neglecting other drivers. In this study, we investigate how fetch and natural surfactants modulate air-sea carbon dioxide exchange. Measurements from the central Baltic Sea show that limited fetch and elevated surfactants significantly suppress this exchange. A new parameterisation is provided, improving regional carbon budgets and evaluations of climate solutions.

## 1. Introduction

The ocean is a major sink of carbon dioxide ($CO_2$) emitted by human activities, substantially mitigating climate change (Friedlingstein et al., 2025). Beyond its natural carbon uptake capacity, marine-based carbon dioxide removal (mCDR) has emerged as a climate mitigation approach under ongoing global warming (Doney et al., 2024). Accurate quantification of global ocean carbon flux and the regional mCDR efficiency is essential for climate predictions. Air-sea $CO_2$ flux is often estimated using the bulk formula:

$$F = K_{660}\left(\frac{Sc}{660}\right)^{-n}(\alpha_w f\mathrm{CO}_{2w} - \alpha_i f\mathrm{CO}_{2a}) \quad (1)$$

where $F$ (e.g., mmol $m^{-2}$ $day^{-1}$) is the air-sea $CO_2$ flux, $K_{660}$ (cm $h^{-1}$) is the gas transfer velocity normalized to a Schmidt number ($Sc$) of 660, corresponding to $CO_2$ in seawater at 20°C. The value of the exponent $n$ is between 1/2 and 2/3 (Jähne et al., 1987), and is often assumed to be 1/2 in the ocean environment (Wanninkhof et al., 2009). $CO_2$ solubilities (e.g., mol $L^{-1}$ $atm^{-1}$) at the base of the mass boundary layer and at the air-sea interface are $\alpha_w$ and $\alpha_i$, respectively. $CO_2$ fugacity ($fCO_2$, µatm) at these locations is $fCO_{2w}$ and $fCO_{2a}$. $Sc$ and $\alpha$ depend on water temperature and salinity (Wanninkhof, 2014; Weiss, 1974). Notably, if both the $CO_2$ flux and $fCO_2$ are known, $K_{660}$ can be derived.

Equation 1 highlights the central role of $K_{660}$ as the kinetic forcing parameter in air-sea $CO_2$ exchange. $K_{660}$ is directly driven by near-surface turbulence (Garbe et al., 2014). On a global scale, wind forcing has a dominant effect on gas transfer velocity, and other factors, such as friction

velocity, waves, and bubbles, are strongly linked with wind speed (Wanninkhof et al., 2009). Thus, the readily available 10-meter neutral wind speed ($U_{10N}$) is often used as the sole variable for parameterising $K_{660}$ (e.g., Ho et al., 2006; Nightingale et al., 2000; Wanninkhof, 2014). However, wind is not the only factor driving gas exchange, as other factors not fully linked to wind speed can substantially influence this exchange at regional scales, particularly in the coastal ocean (Upstill-Goddard, 2006). Existing $U_{10N}$-based $K_{660}$ formulations in the Baltic Sea yield controversial results (e.g., Gutiérrez-Loza et al., 2022; Kuss et al., 2004), highlighting the lack of mechanistic understanding of air-sea gas exchange.

Surfactants are surface-active compounds, molecules, or biomolecules. They are ubiquitous in the ocean and often highly concentrated in coastal waters through biological production and terrestrial inputs (Mustaffa et al., 2020; Sabbaghzadeh et al., 2017; Wurl et al., 2011), suppressing gas exchange by damping surface turbulence and forming an additional diffusion barrier (McKenna and McGillis, 2004; Pereira et al., 2016). In contrast, wave breaking enhances gas transfer, especially for low-soluble gases, by introducing bubbles as an exchange pathway in addition to the interfacial exchange route (Bell et al., 2017; Blomquist et al., 2017; Dong et al., 2025; Woolf, 1997). Wave breaking is strongly impacted by wind fetch (defined as the distance over which wind acts on the water surface), because limited fetch suppresses wave breaking and bubble generation (Fairall et al., 2006; Kunz and Jähne, 2018; Ocampo-Torres and Donelan, 1995; Prytherch and Yelland, 2021; Woolf, 2005). Understanding how these mechanisms influence air-sea gas exchange is essential for regional (coastal) carbon budgets and for developing robust monitoring, reporting, and verification (MRV) frameworks to support mCDR strategies (e.g., Ho et al., 2023).

The Baltic Sea, with its high primary productivity (Schmidt and Schneider, 2011) in summer and limited fetch, provides an ideal natural laboratory to investigate the combined effects of surfactants and fetch on air-sea gas exchange. We therefore conducted a comprehensive gas exchange experiment in the central Baltic Sea to quantify the impact of factors additional to wind speed on gas exchange.

## 2. Methods

### 2.1 CenBASE cruise

The Central Baltic Air-Sea Exchange Experiment (CenBASE; EMB 295) was conducted in summer 2022, immediately after the phytoplankton bloom season, to capture strong air-sea gas exchange signals (Parard et al., 2016; Bittig et al., 2024). The research cruise on the *R/V Elisabeth Mann Borgese* (EMB) departed from Rostock, Germany, on 2 July and returned on 18 July, with the primary study area located in the Gotland Basin (Fig. 1A).

Eddy covariance (EC) $CO_2$ flux observations (Section 2.2) and the $^3He/SF_6$ dual-tracer experiment (see Appendix A1) were performed simultaneously to determine gas transfer velocities, representing the second successful joint deployment of these two approaches after GasEx-98 (Ho and Wanninkhof, 2016; McGillis et al., 2001). Surfactant samples were collected from both the microlayer and underlying water (see Appendix A2). Wave parameters were extracted from the ERA5 hourly reanalysis data product (0.5° × 0.5°) (Hersbach et al., 2020) based on the cruise track's spatiotemporal coordinates. Additional measurements included $fCO_2$, sea surface properties, and meteorological variables to support the analysis.

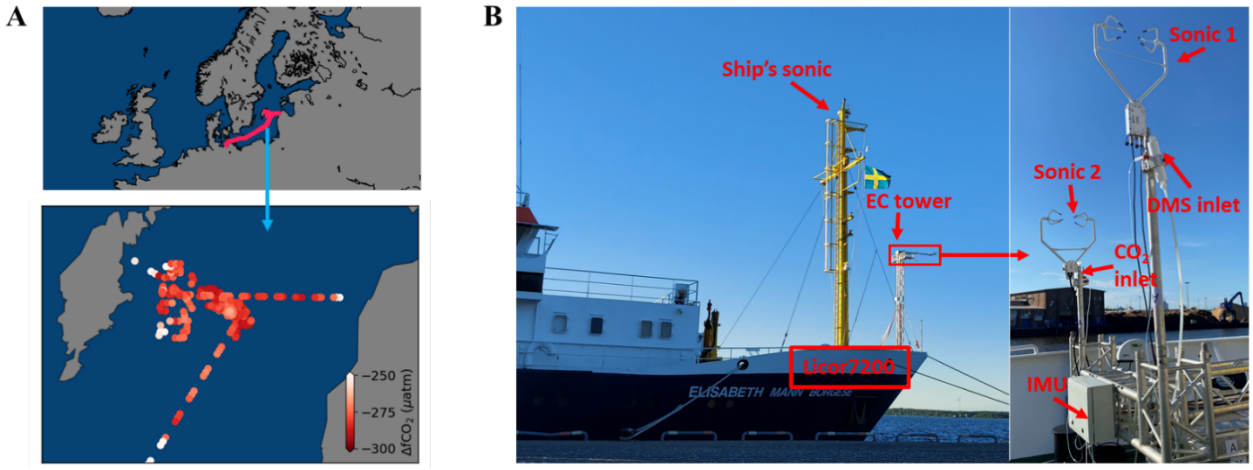


**Figure 1: CenBASE cruise tracks and the ship-based eddy covariance (EC) system.** Left panel: Cruise tracks in the central Baltic Sea, color-coded by air-sea $CO_2$ fugacity differences ($\Delta fCO_2$). Middle panel: Research vessel EMB during the CenBASE cruise; a custom-built EC tower is mounted at the bow. Right panel: Instruments mounted on top of the tower, including sonic anemometers, a motion sensor (IMU), and the $CO_2$ inlet. Additional setup details are provided in Section 2.

## 2.2 Eddy covariance $CO_2$ flux measurements

The EC technique allows for direct measurements of air-sea $CO_2$ flux using the following equation:

$$F = \rho\overline{w'c'} \quad (2)$$

where $\rho$ is the mean molar density of dry air (e.g., in mole $m^{-3}$), $w$ is the vertical wind velocity (in m $s^{-1}$), and $c$ is the dry air mole fraction of $CO_2$ (in ppm or μmol $mol^{-1}$). The primes denote the fluctuations from the mean, and the overbar indicates time averaging. Due to the dynamic nature of the marginal sea environment, a 10-minute averaging interval was chosen, shorter than the 20-30 minutes typically used in the open ocean (e.g., Blomquist et al., 2017). The $CO_2$ transfer velocity ($K_{660\_CO2}$) is derived by combining Equations 1 and 2. The EC momentum flux is similarly calculated as $\rho\overline{w'u'}$, where $u$ is the horizontal wind component. The friction velocity ($u_*$) is then derived as the square root of the momentum flux magnitude.

Most components of the EC system were mounted on a custom-built tower at the bow of the ship to minimize the flow distortion (Fig. 1B). The tower extended 5 m above the deck, reaching a height of 14 m above mean sea level (MSL). A three-dimensional (3D) sonic anemometer (CSAT3B, *Campbell Scientific*) was installed on the starboard arm to measure the wind fluctuations, with a backup unit on the port side (CSAT3). An Inertial Measurement Unit (IMU, *SBG Systems*), housed in a meteorological box at the top of the tower, recorded ship motion. The IMU was positioned 66 cm from the starboard sonic and 173 cm aft of it. $CO_2$ fluctuations were measured using a LI-7200 gas analyzer. The sampled air was dried with a Nafion dryer operating in 'reflux' mode (Perma Pure LLC, 2024). Air was drawn from the port-side inlet through a ~10-m Teflon tube (3/8" inner diameter) at a stable flow rate of 33.2 ± 0.3 L $min^{-1}$, which results in turbulent flow within the tube. The 20-Hz signal from the sonic anemometer, IMU, and LI-7200 was logged by a datalogger (CR6, *Campbell Scientific*).

Data processing and quality control procedures followed those described in Dong et al. (2021). Briefly, motion corrections were applied to the wind (Edson et al., 1998; Miller et al., 2008) and $CO_2$ signals (Miller et al., 2010) to remove contamination from ship motion. A nitrogen puff test revealed a 0.3 s e-folding response time, which is used to correct the high-frequency attenuation (Blomquist et al., 2014). The time delay (~2.5 s) between the inlet and the gas analyzer was assessed via the maximum covariance method. Flow distortion was minimized by mounting the EC tower arms beyond the ship's hull.

### 2.3 Auxiliary observations

The partial pressure of $CO_2$ in surface water was measured at 1-minute intervals using the Mobile Equilibrator Sensor System (MESS) paired with two off-axis integrated cavity output laser spectrometers (oa-ICOS, Los Gatos Instruments) (Sabbaghzadeh et al., 2021). Seawater was continuously drawn from the ship's inlet at a depth of ~3.3 m. Atmospheric $CO_2$ was measured daily using an air inlet mounted on the ship's foremast at 13.5 m above MSL. These air $CO_2$ data are compared to the absolute $CO_2$ values measured by the EC gas analyzer (LI-7200, LI-COR, Inc.) to generate the 10-min time series of atmospheric $CO_2$. Sensor calibration was performed almost daily using standard gases from the Central Analytical Laboratories of the European Integrated Carbon Observation System (ICOS RI). Mean wind measurements were obtained from a sonic anemometer mounted 17 m above MSL on the ship's foremast to minimize flow distortion (O'Sullivan et al., 2013). Residual distortion was corrected using the ERA5 reanalysis wind product and nearby station records (see Appendix A3). Atmospheric pressure and temperature at ~13.5 m MSL were recorded by the onboard weather station. Surface seawater temperature and salinity were monitored by the ship's underway system and calibrated against CTD (conductivity, temperature, and depth) casts. A spar buoy equipped with cameras, temperature, salinity, and dissolved oxygen sensors was deployed at several stations to characterize upper-ocean bubble and water column dynamics.

In addition, EC air-sea $CO_2$ flux observations from previous open-ocean cruises (Yang et al., 2022) are also used to comparison with the CenBASE results. Wave parameters were extracted from the ERA5 analysis wave product according to these open-ocean EC cruise tracks (see Yang et al., 2022) and the CenBASE cruise. The COARE model is used to estimate the bulk $u_*$ (Edson et al., 2013). For the open-ocean scenario, environmental variables from the corresponding cruises are used as inputs to the COARE model (Yang et al., 2022). The environmental parameters observed during the CenBASE cruise are used to estimate the Baltic Sea $u_*$ in the COARE model.

## 3. Results

### 3.1 Environmental variables and the $CO_2$ flux

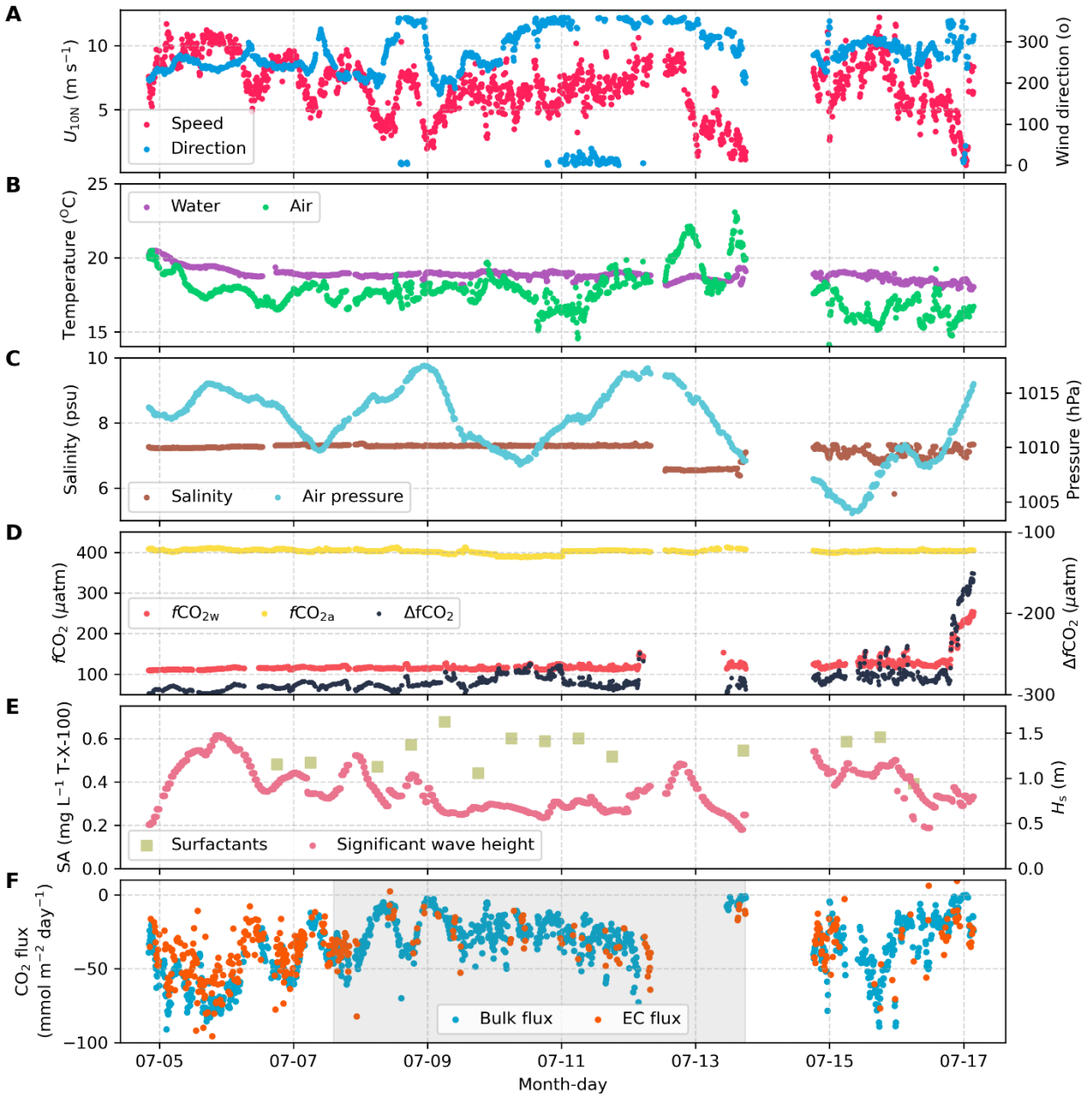


**Figure 2: Ten-minute averages of environmental variables and air-sea $CO_2$ flux. A**: Neutral 10-meter wind speed ($U_{10N}$, red) and wind direction (blue). **B**: Surface seawater temperature (purple) and air temperature (green). **C**: Seawater salinity (brown) and sea-level air pressure (light-blue). **D**: $CO_2$ fugacity in surface seawater (red) and atmosphere (yellow), and their difference ($\Delta fCO_2$, black). **E**: Surface microlayer surfactant activity (SA, light green squares) and significant wave height extracted from ERA5 ($H_s$, red); **F**: Bulk $CO_2$ flux estimates (blue, based on $K_{660}$ parameterisation from Ho et al., 2006) and EC $CO_2$ flux observations (orange). The dual-tracer tracing period is indicated by the light gray shading. Data are missing from 12-14 July due to a medical event and a temporary shortage of liquid nitrogen, which required the vessel to leave the primary study area.

During CenBASE, winds predominantly originated from the west to north sector (Fig. 2A), with an effective fetch of approximately 50-300 km in the main study area (Fig. A1, Appendix). The wind speed ranged from 1 to 12 m $s^{-1}$ (Fig. 2A). Water depth across the central Baltic Sea study site ranged from ~50 to 250 m. Surface water was generally warmer than the overlying air (Fig. 2B), resulting in an unstable boundary layer. Surface salinity remained consistent at approximately 7.3 throughout the study region (Fig. 2C). The cruise took place shortly after a summer phytoplankton bloom, resulting in remarkably low sea surface $fCO_2$ (~120 µatm; Fig. 2D). Atmospheric $fCO_2$ remained constant at ~403 µatm, creating a strong air-sea gradient ($\Delta fCO_2 \approx$ -280 µatm on average; Fig. 2D) that generated strong ocean $CO_2$ uptake signals.

Surface microlayer surfactant activity (SA), expressed as Triton-X-100 equivalents, was relatively constant at 0.54 ± 0.08 mg $L^{-1}$ (Fig. 2E), significantly higher than typical open-ocean values (0.1-0.2 mg $L^{-1}$; Mustaffa et al., 2020; Sabbaghzadeh et al., 2017). Modeled significant wave height ($H_s$) remained below 1.5 m (Fig. 2E), lower than expected for comparable wind speeds in the open ocean (Fig. A2). Bulk $CO_2$ fluxes estimated from the measured $\Delta fCO_2$ and an open-ocean dual-tracer $K_{660}$ parameterisation (Ho et al., 2006) were higher than observed EC fluxes under high wind speeds and lower than observed EC fluxes under low wind speeds (Fig. 2F and Fig. A3). During the tracer-tracking period (8-14 July), frequent ship heading changes reduced EC flux quality, leading to most valid EC measurements being obtained from outside this period (Fig. 2F, light-gray shading). Nevertheless, as both EC and dual-tracer were collected in the same study area, the $K$ from both methods can be reasonably considered simultaneous measurements.

### 3.2 Friction velocity

The friction velocity is a key parameter characterizing near-surface turbulence. Observed values of $u_*$ from EC momentum fluxes during CenBASE were 10% higher than modelled open ocean $u_*$ at the same wind speeds (Fig. 3A), likely reflecting fetch-related differences. The wave field in the central Baltic Sea is much younger than in the open ocean, with wave age ~60% lower at the same wind speed (Fig. 3B). The waves are shorter and steeper than in the open ocean (Fig. A2). This wave field enhances sea surface roughness and elevates $u_*$ relative to the open sea. $u_*$ predicted by the COARE3.6 model, when forced with observed environmental and extracted wave parameters during CenBASE, broadly agrees with measurements (Fig. 3A). This suggests that the COARE model remains applicable in fetch-limited marine environments when wave information is

included, despite being developed primarily from open-ocean observations (Edson et al., 2013). Given that $u_*$ is an indicator of surface wind-induced turbulence, this elevated $u_*$ is expected to enhance $CO_2$ transfer velocity (see Section 3.4).

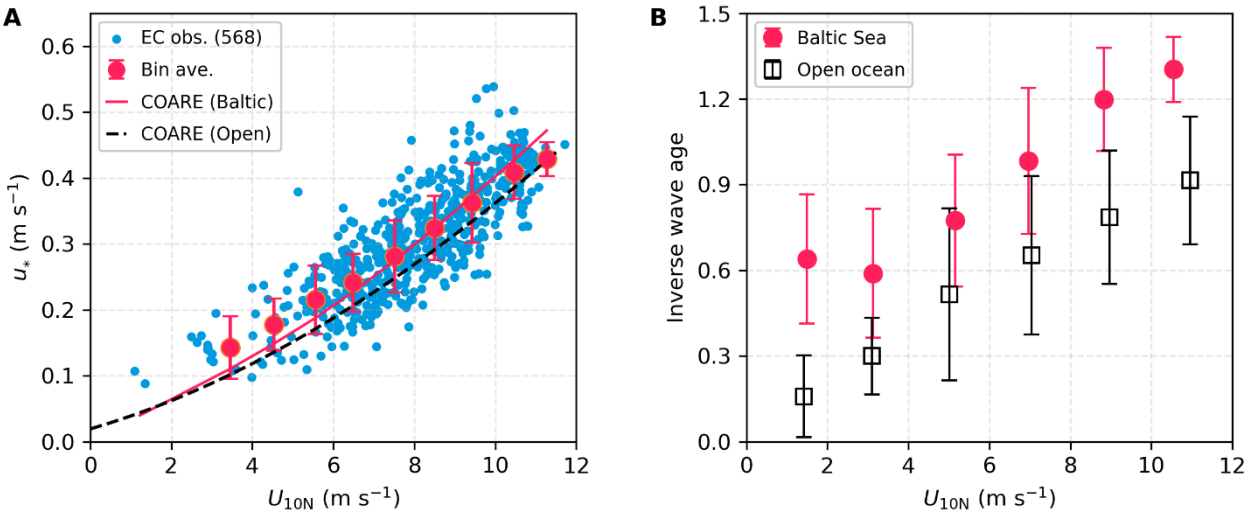


**Figure 3: Friction velocity ($u_*$) and inverse wave age in the Baltic Sea (CenBASE) and open ocean. A**: $u_*$ derived from EC air-sea momentum fluxes versus 10-meter neutral wind speed ($U_{10N}$). Blue dots: 10-min $u_*$ observations during CenBASE (568 points), with red points corresponding to bin averages (per 1 m s$^{-1}$). Red line: $u_*$ simulated by COARE3.6 using the Baltic Sea environmental data; Black-dashed line: COARE3.6 simulations in the open ocean. **B:** Inverse wave age ($U_{10N}$/ $C_p$) in the Baltic Sea (red dots) and open ocean (black squares). Error bars denote ± 1 standard deviation (STD) of bin averages. The hourly wave parameters are shown in Fig. A2 of the Appendix.

### 3.3 Gas transfer velocities from EC and DT

The $CO_2$ transfer velocity ($K_{660\_CO2}$) was derived from EC air-sea $CO_2$ flux and $\Delta fCO_2$ observations using Equation 1. After quality control, 301 valid 10-min $K_{660\_CO2}$ data points were retained (Fig. 4). The large $|\Delta fCO_2|$ (~280 µatm) ensured accurate $K_{660\_CO2}$ derivations, with hourly uncertainties of ~20% (Fig. A4), substantially lower than typical cruise-based uncertainties (e.g., ~30% during the HiWinGS cruise; Blomquist et al., 2017). The cool skin correction (reduces $\Delta fCO_2$ by ~2 µatm; Woolf et al., 2016) is negligible relative to the observed $\Delta fCO_2$ and was therefore ignored. $K_{660}$ from the DT experiment is summarized in Appendix A1.

The EC dataset offers high temporal resolution (~10 min), enabling investigation of small-scale processes influencing gas exchange. The EC observations span a broad range of wind speeds (1 to 12 m $s^{-1}$, Fig. 4A), providing a robust constraint of $K_{660\_CO2}$ under low-to-moderate wind conditions. In contrast, DT-derived $K_{660}$ represents daily averages, in which short-term extremes (i.e., low and high wind conditions) are smoothed, resulting in seven observations concentrated at $U_{10N}$ of 5-9 m $s^{-1}$ (Fig. 4A). Within this wind range, DT-and EC-derived $K_{660}$ values are in good agreement, with the former on average being only slightly (~8%) lower than the latter (Fig. 4).

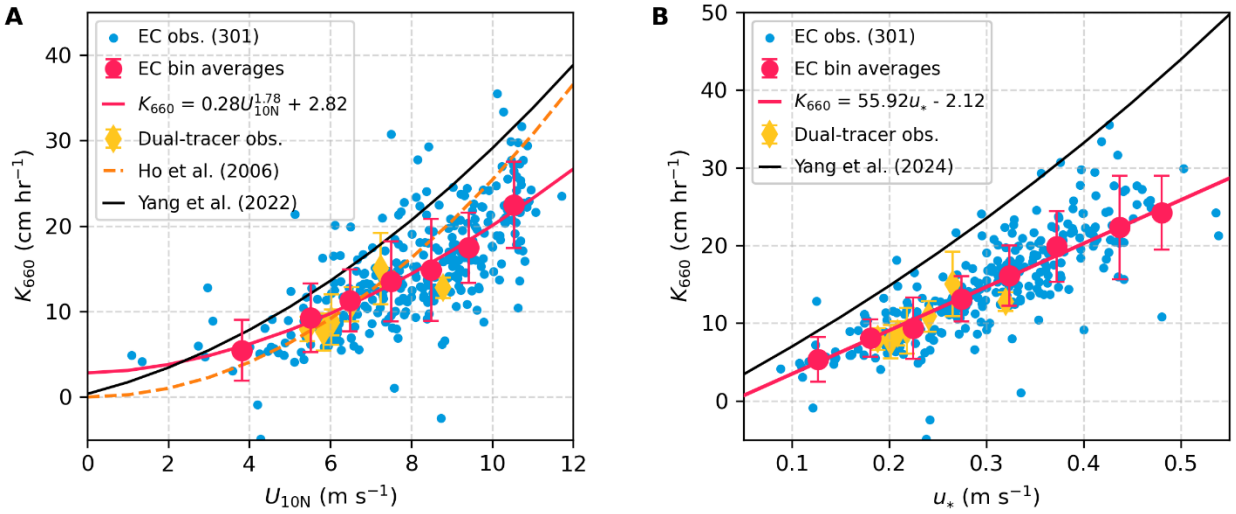


**Figure 4: Gas transfer velocity ($K_{660\_CO2}$) in the central Baltic Sea during the CenBASE cruise. A**: Relationships between $K_{660}$ and $U_{10N}$. **B**: Relationships between $K_{660}$ and observed $u_*$. Blue dots in both panels represent 10-min $K_{660\_CO2}$ (N = 301), with red dots denoting bin averages (1 m $s^{-1}$ $U_{10N}$ bins or 0.05 m $s^{-1}$ $u_*$ bins) ± 1 STD. Red lines indicate the fit to the bins, with $R^2$ of 0.48 for the fit with $U_{10N}$ and 0.59 for the fit with $u_*$. Yellow diamonds show dual-tracer (DT) transfer velocities ($K_{660\_3He/SF6}$) measured concurrently with EC (Dobashi et al., submitted). The orange line in panel A denotes the open ocean DT-based parameterisation from Ho et al. (2006). The black lines in panels A and B correspond to the open-ocean EC-based parameterisations of Yang et al. (2022; $U_{10N}$-dependent) and Yang et al. (2024; $u_*$ and sea-state dependent), respectively.

DT-derived $K_{660}$ values during CenBASE also generally agree with the open-ocean DT-based parameterisation of Ho et al. (2006) under equivalent wind speeds (orange dashed line in Fig. 4A), with the former on average being only ~7% lower than the latter. However, EC-derived $K_{660\_CO2}$ values deviate systematically from this open-ocean relationship (Ho et al., 2006), being higher at

low wind speeds (1-7 m $s^{-1}$, +12%) and lower at high wind speeds (7-12 m $s^{-1}$, -18%) (Fig. 4A). This divergence does not contradict the agreement between the DT-and EC-based $K_{660}$ observations, as this agreement falls within the 5-9 m $s^{-1}$ range (where the DT data concentrate). Fitting $K_{660\_CO2}$ with $U_{10N}$ reveals a weaker wind speed dependence than the open ocean DT-based parameterisation (Fig. 4A). It is worth noting that including a constant term in the $K_{660\_CO2}$-$U_{10N}$ fitting function (i.e., $K_{660\_CO2} = aU_{10N}^{b} + c$, $R^2$ = 0.48) improves the fit compared to a purely power-law form (i.e., $K_{660\_CO2} = aU_{10N}^{b}$, $R^2$ = 0.42) (Fig. A5), suggesting a non-zero $CO_2$ exchange (~3 cm $hr^{-1}$) under calm conditions. This is unsurprising, since the chemical enhancement (Cole & Caraco, 1998; Fairall et al., 2022; Yang et al., 2022) and likely buoyancy flux sustain $CO_2$ transfer at low wind speeds (McGillis et al., 2004; Wanninkhof et al., 2009).

Notably, the DT data collected during CenBASE provide only limited constraints at wind speeds below 5 m $s^{-1}$ and above 9 m $s^{-1}$, and the $K_{660}$-$U_{10N}$ relationship derived from these data is sensitive to the chosen functional form (Fig. A5). Moreover, the DT-based open-ocean $K_{660}$ estimates are lower than the EC $CO_2$-based estimates across the wind speed range observed during CenBASE (Fig. 4A), likely reflecting differences in methodology. Because the CenBASE DT data have been interpreted in detail by Dobashi et al. (submitted), and, more importantly, because the EC measurements resolve finer-scale processes and ensure methodological consistency, the subsequent section focuses on comparing EC $CO_2$ observations in the Baltic Sea with those EC $CO_2$ observations in the open ocean.

### 3.4 Suppression of air-sea $CO_2$ exchange

The EC-derived $K_{660\_CO2}$ during CenBASE was generally lower than open-ocean EC $CO_2$ transfer velocities (Yang et al., 2022; 2024) (Figs. 4A and 4B), indicating a substantial suppression of $CO_2$ exchange in the Baltic Sea. To explain this reduction, we partition the total gas transfer velocity ($K_{660}$) into interfacial ($K_{i660}$) and bubble-mediated ($K_{b660}$) components (i.e., $K_{660} = K_{i660} + K_{b660}$). $K_{i660}$ is primarily driven by wind stress or $u_*$, whereas $K_b$ depends on both the wind forcing and sea state. A machine-learning analysis of 15 open ocean datasets identified the significant wave height ($H_s$, including both windsea and swell) as a key proxy for sea state that strongly affects $K_{660\_CO2}$ (Yang et al., 2024). Based on this analysis, Yang et al. (2024) express the $K_{660}$ as (Fig. 4B, black line):

$$K_{660} = K_{i660} + K_{b660} = 55u_* + 10u_*H_s \quad (3)$$

Because $K_b$ depends on solubility, normalizing it using the Schmidt number (i.e., converting $K_b$ to $K_{b660}$) may not be strictly appropriate. However, the sensitivities of the $CO_2$ transfer velocity to $Sc^{-1/2}$ and $\alpha^{-1}$ are nearly identical (see Fig. A1 in Dong et al., 2025). Therefore, normalization using either $Sc$ or $\alpha$ produces almost the same gas transfer velocities. For simplicity and consistency, we adopt the $Sc$-based normalization in this study.

The observed EC $K_{660}$ during CenBASE was on average 14.9 cm $hr^{-1}$. To compare this value with open-ocean conditions at equivalent wind speeds, we apply the wind-speed observations from the CenBASE cruise (i.e., wind speed values shown in Fig. 4A) to Equation 3 to estimate open-ocean $K_{660}$, yielding average values of $K_{i660}$ = 15.1 cm $hr^{-1}$, $K_{b660}$ = 7.0 cm $hr^{-1}$, and $K_{660}$ = 22.1 cm $hr^{-1}$. This means that the observed $K_{660}$ during CenBASE was 33% (7.2 cm $hr^{-1}$) lower than the open-ocean $K_{660}$ estimate.

Equation 3 implies a linear dependence of $K_{660\_CO2}$ on $u_*$. Regression of the observed $K_{660\_CO2}$ against $u_*$ indeed yields an approximately linear relationship (Fig. 4B), consistent with prior findings at low-to-moderate winds (Landwehr et al., 2018; Yang et al., 2022). Additionally, the $K_{660\_CO2}$-$u_*$ fit ($R^2$ = 0.59) outperforms the $K_{660\_CO2}$-$U_{10N}$ fit ($R^2$ = 0.48), confirming that $u_*$ better captures variability in gas transfer velocity than $U_{10N}$ (Jähne et al., 1987; Landwehr et al., 2018; Yang et al., 2022). As shown in Fig. 3A, the observed $u_*$ during CenBASE was ~10% higher than open-ocean values under equivalent wind speeds, implying a ~10% enhancement in $K_{660\_CO2}$ due to fetch-related increases in shear stress (Vickers and Mahrt, 1997). It is important to note that the observed 33% reduction in $K_{660\_CO2}$ includes this enhancement, suggesting that $CO_2$ exchange was suppressed even more, by ~43% (9.2 cm $h^{-1}$) relative to open-ocean conditions.

According to Equation 3, $K_b$ is linearly dependent on $H_s$. Due to the limited fetch, the $H_s$ during CenBASE was 57% lower than in the open ocean at the equivalent $u_*$ (Fig. 5A, Table 1), and this reduction is expected to cause a comparable decrease in $K_b$. Using the extracted $H_s$ values from ERA5 for CenBASE, the parameterised $K_{b660}$ decreases on average from 7.0 cm $hr^{-1}$ to 4.0 cm $hr^{-1}$, corresponding to an 18% suppression on the total $K_{660\_CO2}$ (Fig. 5B; Table 1), explaining about half of the observed suppression during CenBASE.

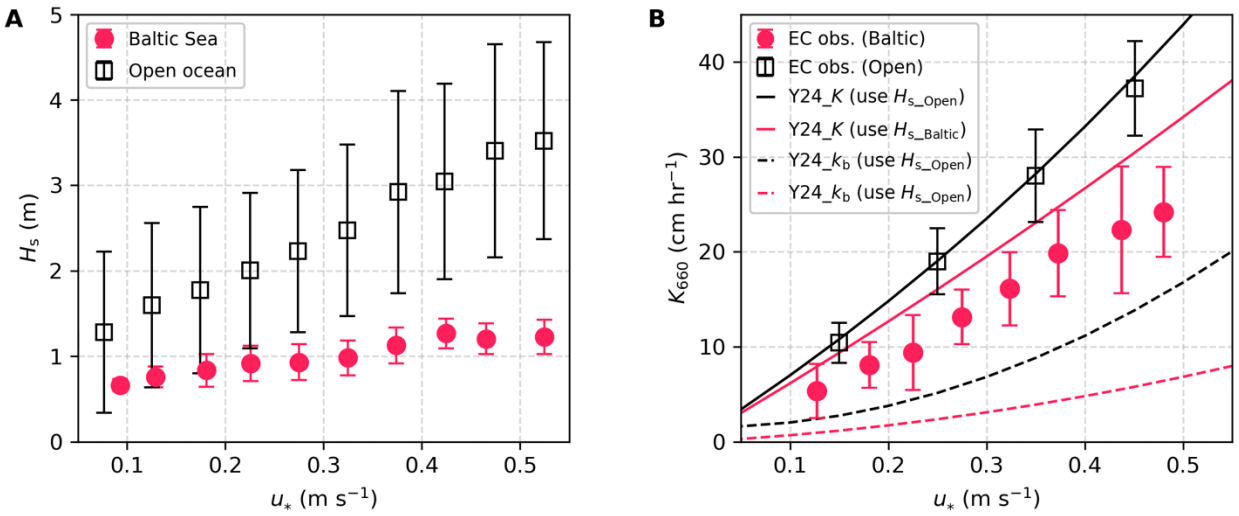


**Figure 5: Comparison of significant wave height ($H_s$) and $K_{660\_CO2}$ between the Baltic Sea and the open ocean. A:** $H_s$ in the Baltic Sea during CenBASE (red dots) and in the open ocean (black squares), with error bars representing ± 1 STD. The data are extracted from ERA5 according to the EC cruise tracks (Yang et al., 2022) and the CenBASE cruise track. **B:** $K_{660\_CO2}$ observations in the Baltic Sea during CenBASE (red dots, the same as the red dots in Fig. 4B) and in the open ocean (black squares, Yang et al., 2022). The black and red solid lines correspond to the parameterised total $CO_2$ transfer velocity (i.e., $K_{660\_CO2}$ from Equation 3; Yang et al., 2024) using the openocean and the Baltic Sea $H_s$, respectively. The black and red dashed lines denote the parameterised bubble-mediated transfer component ($K_{b660}$; Equation 3) using the open ocean and the Baltic Sea $H_s$, respectively.

Surfactants inhibit both interfacial (e.g., Frew, 1997) and bubble-mediated gas exchange (e.g., Woolf, 1993), and their concentrations in the Baltic Sea are substantially higher than in the open ocean. We assume that all residual suppression of $K_{660\_CO2}$ during CenBASE, which cannot be explained by fetch effects, is caused by surfactants. Under this assumption, the residual 25% suppression (i.e., 5.4 cm hr$^{-1}$; Fig. 5B and Table 1) reflects the impact of elevated surfactant levels. This effect is not captured by the Yang et al. (2024) parameterisation, which is based primarily on open-ocean observations characterized by low surfactants (Wurl et al., 2011; Fig. A6).

The resulting suppression fraction (*sf*) is consistent in magnitude with previous field-based estimates (Fig. 6; Mustaffa et al., 2020; Salter et al., 2011; Yang et al., 2021) within uncertainty (see Section 3.5). The constrained *sf* is generally smaller than laboratory-derived values (Fig. 6A), likely due to challenges in extrapolating laboratory conditions to the field. Notably, previous

studies report conflicting relationships between *sf* and surfactant concentration. Some show increasing *sf* with increasing concentration (Mesarchaki et al., 2015; Pereira et al., 2018; Ribas-Ribas et al., 2018), whereas others identify a threshold concentration above which *sf* shows little change (Mustaffa et al., 2020; Schmidt and Schneider, 2011) (Fig. 6A). Because surfactant concentrations were nearly constant during CenBASE, we cannot assess this relationship here.

Several studies also show that *sf* decreases with wind speed (Fig. 6B; Bock et al., 1999; Mesarchaki et al., 2015; Salter et al., 2011; Yang et al., 2021), and the *sf* constrained here aligns well with these findings, especially those from field observations. Fitting *sf* as a function of $u_*$ yields a correction factor (i.e., 1 – *sf*) that can be applied to Equation 3 to account for surfactant effects, generating the updated parameterisation:

$$K_{660} = (1 - 0.38e^{-1.25u_*})(55u_* + 10u_*H_s) \quad (4)$$

This parameterisation reflects conditions during CenBASE, where the surfactant concentration was relatively stable at ~0.5 mg $L^{-1}$. If a SA concentration-dependent *sf* is needed, one option is the published linear relationship $sf = 0.32SA + 0.025$ (Pereira et al., 2018). However, this formulation maybe physically inconsistent because it predicts a non-zero suppression even when $SA = 0$, whereas *sf* should theoretically approach zero in surfactant-free conditions. To address this, we re-evaluated the same dataset used in the original study (Pereira et al., 2018) and fitted a proportional relationship that passes through the origin: $sf = 0.38SA$. The goodness-of-fit ($R^2$ = 0.49) is only marginally lower than the original relationship (0.51, Pereira et al., 2018), indicating that the proportional form captures the data nearly as well while remaining physically realistic. For the mean CenBASE surfactant concentration ($SA$ = 0.54 mg $L^{-1}$), this relationship yields $sf$ = 0.21. Applying this SA-dependent suppression to the wind-dependent correction in Equation 4 results in the combined parameterisation:

$$K_{660} = \frac{1-0.38SA}{0.79}(1 - 0.38e^{-1.25u_*})(55u_* + 10u_*H_s) \quad (5)$$

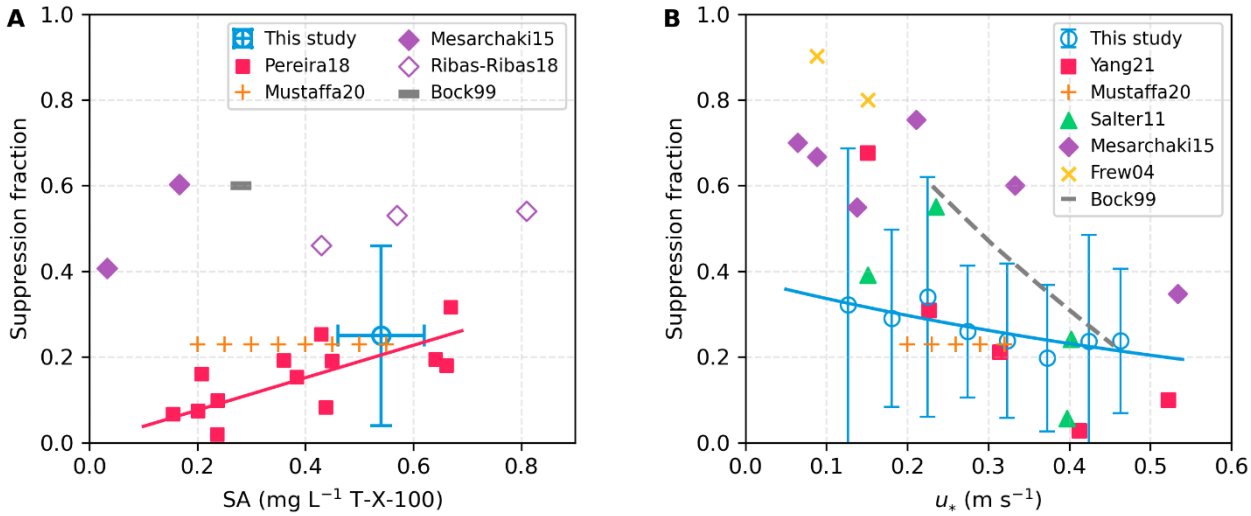


**Figure 6: Surfactant-induced suppression fraction on $K_{660}$ (*sf*) from this study and previous work. A**: *sf* as a function of surfactant concentration under low-moderate wind speeds. The blue circle shows the mean constrained *sf* from this study; horizontal and vertical error bars denote the standard deviation of observed SA and the associated uncertainty of the constrained *sf*. Red squares indicate *sf* from wave-tank experiments with natural Atlantic seawater at wind speeds <13 m s$^{-1}$ (Pereira et al., 2018), with the red line showing the linear fit (*sf* = 38×SA). Orange pluses show *sf* constrained from field $K_{660}$ observations using the chamber technique with natural surfactant (Mustaffa et al., 2020). Diamonds (filled/unfilled) and the grey dash represent wave-tank studies using artificial soluble surfactants (Mesarchaki et al., 2015; Ribas-Ribas et al., 2018; Bock et al., 1999). **B**: *sf* as a function of $u_*$. Blue circles show *sf* constrained from the residual suppression of observed $K_{660\_CO2}$ from this study, with error bars indicating uncertainties. The blue line corresponds to the fit based on the blue circles ($0.38\times e^{1.25u*}$, $R^2 = 0.65$). Red squares represent values derived from an EC-based $CO_2$ transfer velocity study (Yang et al., 2021). Orange pluses denote the Mustaffa et al. (2020) dataset with surfactant concentrations of 0.2-0.6 mg L$^{-1}$. Green triangles show *sf* inferred from EC-based DMS and DT exchange experiments in artificial insoluble surfactant patches (Salter et al., 2011). Purple diamonds represent Mesarchaki et al. (2015), who used ~0.2 mg L$^{-1}$ of artificial soluble surfactant. Yellow crosses indicate *sf* derived from coastal heat transfer measurements (Frew et al., 2004). The grey dashed line shows laboratory experiments with artificial soluble surfactants at ~0.3 mg L$^{-1}$ (Bock et al., 1999).

Previous studies have suggested that water-side convection may influence gas exchange in both open-ocean (McGillis et al., 2004) and Baltic conditions (Rutgersson and Smedman, 2010). During CenBASE, a small spar buoy recorded oxygen, temperature, and salinity at depths of 1.2 m and

2.9 m. Dissolved oxygen exhibited small-scale variability with similar patterns at both depths (Fig. A7), indicating coherent near-surface structure over 5-20 m scales, likely driven by wind-induced turbulence intermittently exposing surface patches to the atmosphere. In contrast, no corresponding variability was observed in temperature or salinity (Fig. A7), suggesting that convection played a negligible role in gas exchange under the observed conditions. This supports our assumption that the deviation in $K_{660\_CO2}$ between the Baltic Sea and the open ocean can be fully attributed to the combined effects of limited fetch and elevated surfactant levels.

### 3.5 Uncertainty analysis

The quantification results shown above are not free from uncertainty. First, we use the $K_b \propto u_* H_s$ relationship for the bubble component, which fits best with the EC-based $K_{660\_CO2}$ observations (Yang et al., 2024). However, alternative formulations have been proposed, such as $K_b \propto u_*^{1.67} H_s^{0.67}$ (Deike and Melville, 2018) and $K_b \propto u_*^{0.9} H_s^{0.9}$ (Brumer et al., 2017a; Fairall et al., 2022). These different exponents indicate that the relative contributions of $u_*$ and $H_s$ to gas exchange may vary slightly, introducing parameterisation uncertainty. Yang et al. (2024) reported that the $R^2$ for the fit (i.e., Equation 3) is ~0.75, indicating that ~25% of the variance in the observed $K$ remains unexplained by the parameterisation. We therefore assign a 25% uncertainty to the parameterisation given in Equation 3. This uncertainty propagates through the suppression estimates. For instance, the uncertainty in the $u_*$-related $K$ enhancement estimate is approximately 0.6 cm hr$^{-1}$ (i.e., 2.2 cm hr$^{-1}$ × 25%). The suppression analysis uses $H_s$ data derived from ERA5 reanalysis, which likely carries an uncertainty of about 30% in the Baltic Sea (Giudici et al., 2023). Consequently, the uncertainty in the $H_s$-related suppression estimate is ~1.6 cm hr$^{-1}$ (i.e., $\sqrt{(4.0 \times 25\%)^2 + (4.0 \times 30\%)^2}$ cm hr$^{-1}$). The uncertainty associated with the surfactant-related suppression is substantially larger because it is not directly determined but inferred as a residual after accounting for other components. Combining the propagated uncertainties from the parameterised total $K$ and from two fetch-induced suppression estimates yields an uncertainty of 5.8 cm hr$^{-1}$ (i.e., $\sqrt{(22.1 \times 25\%)^2 + 0.6^2 + 1.6^2}$ cm hr$^{-1}$), corresponding to approximately 110% of the estimated suppression value (Table 1).

Furthermore, it is worth noting that the two corrections in Equation 5 (i.e., the *SA*-*sf* correction and the $u_*$-*SA* correction) are implicitly assumed to be independent. However, potential interactions between $u_*$-dependent *SA* variation and the *SA* influence on *sf* may introduce additional uncertainty into Equation 5.

**Table 1.** Comparison of mean gas transfer velocities between measurements in the Baltic Sea and estimates using the open ocean parameterisation from Yang et al. (2024) under identical wind speed conditions (Equation 3). The percentages in parentheses in the $K_i$, $K_b$, and $K$ columns indicate the relative difference between the Baltic Sea and the open ocean. The last column is the uncertainty assessment of the values in the $K$ column with the values in parentheses representing the relative uncertainties. The positive (negative) sign represents the enhancement (suppression).

| | | | $K_{i660}$ (cm hr$^{-1}$) | $K_{b660}$ (cm hr$^{-1}$) | $K_{660}$ (cm hr$^{-1}$) | Uncertainty (cm hr$^{-1}$) |
|---|---|---|---|---|---|---|
| Open ocean (model) | | | 15.1 | 7.0 | 22.1 | ± 5.5 (± 25%) |
| Impact factors (model) | Fetch | $u_*$ | +1.5 (+10%) | +0.7 (+10%) | +2.2 (+10%) | ± 0.6 (± 25%) |
| | | $H_s$ | 0 | -4.0 (-57%) | -4.0 (-18%) | ± 1.6 (± 40%) |
| | Surfactants | | Unsure | Unsure | -5.4 (-25%) | ± 5.8 (± 107%) |
| Baltic Sea (CenBASE, EC) | | | - | - | 14.9 (-33%) | - |

### 3.6 Implications for Baltic Sea $CO_2$ flux estimates

The CenBASE cruise took place during the summer bloom (July), when chlorophyll *a* (Chl-*a*) is high (Pitarch et al., 2016) and $fCO_{2w}$ is strongly reduced by primary productivity (e.g., Parard et al., 2016; Bittig et al., 2024). To upscale these results, we adopt a $fCO_{2w}$ product from Bittig et al. (2024) to examine how fetch and surfactants shape the climatological $CO_2$ flux of the Baltic Sea. This climatological $fCO_{2w}$ product is derived by combing observations and model patterns. The $fCO_{2w}$ indicates a $CO_2$ sink in summer and a source in winter (Fig. 7A). However, weaker summer winds and stronger winter winds suggest that the magnitudes of uptake and outgassing may be similar. Seasonal cycles of $u_*$ and $H_s$ closely follow wind speed (Fig. 7B), while Chl-*a* peaks during the spring-summer bloom and remains low in winter (Fig. 7C). We estimate monthly surfactant concentrations by scaling the July CenBASE value (0.54 mg L$^{-1}$) with monthly Chl-*a* concentrations following the idea of Wurl et al. (2011) and using the formula 0.54×Chl-*a*/Chl-

$a_{\_July}$ mg $L^{-1}$. Equation 5 is then used to compute the corresponding suppression of gas transfer, $1-\frac{1-0.38SA}{0.79}(1-0.38e^{-1.25u_*})$. The resulting *sf* reflects the seasonal Chl-*a* cycle and modulations by $u_*$, yielding ~25% suppression in summer and ~10% in winter (Fig. 7C). However, surfactant concentrations are not solely determined by Chl-*a*; for example, humic acids also act as surfactants (e.g., Klavins & Purmalis, 2010), and the Baltic Sea is known for elevated humic acid levels due to significant terrestrial inputs (Hammer et al., 2017). Therefore, estimating surfactant levels based solely on the basis of Chl-*a* has inherent limitations.

We estimate $K_{660}$ using three parameterisation schemes: the conventional open ocean DT-based $U_{10N}$ formulation (Ho et al., 2006), the open ocean EC $CO_2$-based $u_*$-$H_s$ formulation (Equation 3; Yang et al., 2024), and the Baltic Sea EC $CO_2$-based $u_*$-$H_s$-*SA* formulation (Equation 5). Although all these schemes reproduce similar seasonal patterns, their magnitudes differ (Fig. 7D), reflecting sea state and surfactant effects as well as the methodological differences. The $u_*$-$H_s$-*SA* parameterisation yields lower values than the $u_*$-$H_s$ scheme because it incorporates surfactant-induced suppression from the surfactant. This suppression is especially strong in summer when SA concentrations are highest, leading to the largest discrepancies of the estimated climatological $K_{660}$ from the $u_*$-$H_s$-*SA* and the $u_*$-$H_s$ schemes. As shown in Section 3.4, $K_{660}$ during CenBASE has been reduced by 33%. Notably, this reduction is relative to open-ocean EC-based estimates. When compared with the open ocean DT-based $U_{10N}$ formulation, however, this reduction occurs only at wind speeds above ~7 m $s^{-1}$. At lower wind speeds, the EC-based $K_{660}$ observations during CenBASE exceed the DT-based estimates (Fig. 4A). Because climatological Baltic Sea wind speeds are typically below 7 m $s^{-1}$ in Spring, Summer, and Autumn (Fig. 7A), the $u_*$-$H_s$-*SA* parameterisation produces higher $K_{660}$ than the $U_{10N}$ formulation in these seasons. In winter, despite higher wind speeds, the $u_*$-$H_s$-*SA* scheme still exceeds the $U_{10N}$-based estimates due to the modulation of the surfactants. The *SA* concentration in winter is estimated to be three times lower than during the summer CenBASE cruise (Fig. 7C), resulting in much weaker suppression.

Overall, relative to the conventional $U_{10N}$ formulation (Ho et al., 2006), the $u_*$-$H_s$-*SA* parameterisation increases $K_{660}$ in all seasons, enhancing both summer $CO_2$ uptake by ~10% and winter outgassing by ~30%, and amplifying the seasonal cycle by ~40%. These opposing seasonal effects are expected to largely compensate, resulting in only a modest change in the annual mean $CO_2$ flux.

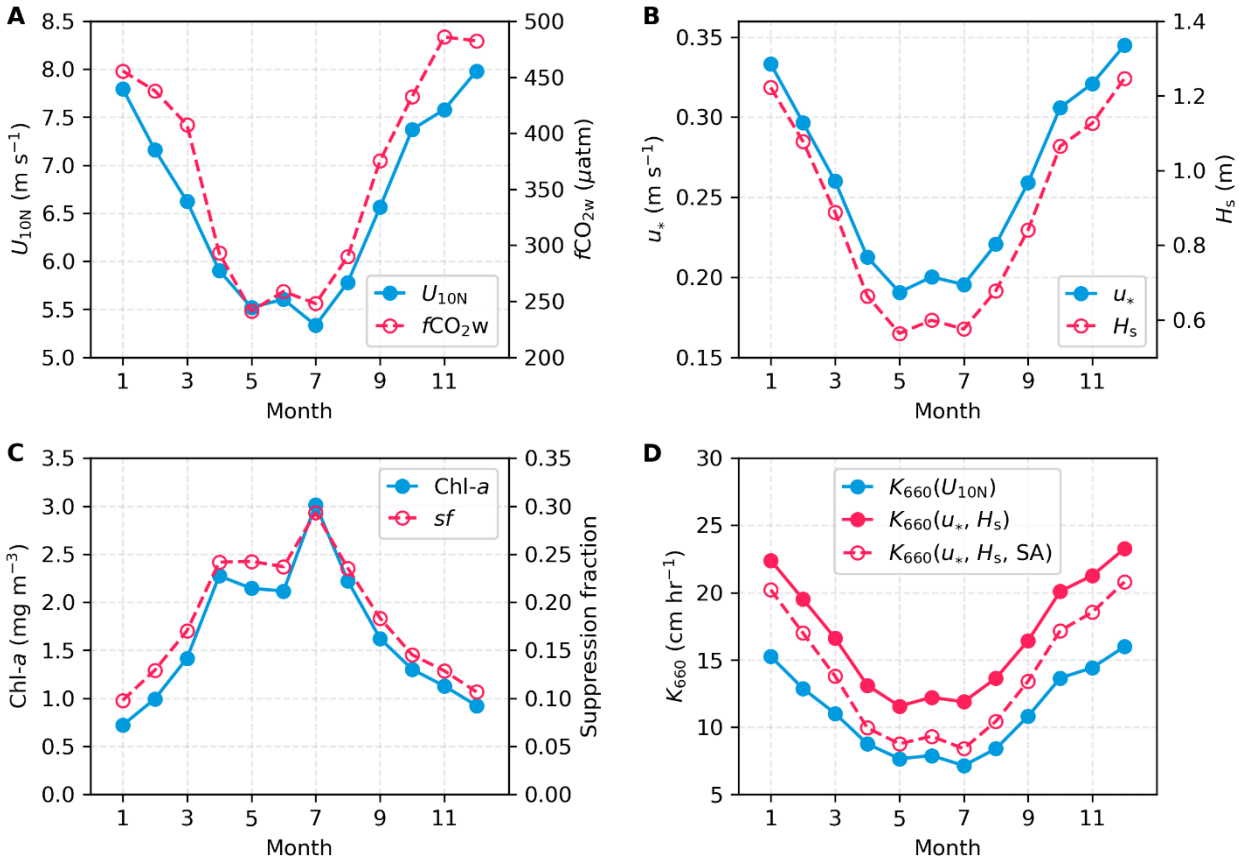


**Figure 7: Climatological seasonal variations of environmental variables and gas transfer velocities in the Baltic Sea. A**: $U_{10N}$ (blue) and $fCO_{2w}$ (red; Bittig et al., 2024). **B**: $u_*$ (blue) and $H_s$ (red). $U_{10N}$, $u_*$, and $H_s$ are averaged from the ERA5 monthly reanalysis data product (Hersbach et al., 2020) for 1998-2018. **C**: Surfactant concentrations scaled from monthly chlorophyll-*a* (Chl-*a*) (Pitarch et al., 2016) and surfactant-induced suppression fraction of $K_{660}$ based on the *SA*- and $U_{10}$-dependent parameterisation (Equation 5). **D**: $K_{660}$ estimated from different parameterisations: $U_{10N}$-based (blue; Ho et al., 2006), $u_*$-$H_s$-based (red solid; Equation 3, Yang et al., 2024); $u_*$-$H_s$-*SA*-based (red dashed; Equation 5).

## 4 Discussion and conclusions

A robust understanding of air-sea gas exchange mechanisms is fundamental for accurately quantifying $CO_2$ fluxes, which is essential for accurate carbon budgets and climate projections. Most previous studies have focused on the open ocean, where $K_{660}$ is typically parameterised as a function of wind speed. In contrast, marginal seas such as the Baltic Sea exhibit more complex

dynamics due to limited fetch and abundant surfactants, which modulate the wind speed dependence of gas exchange. To investigate these processes, a dedicated experiment was conducted in the central Baltic Sea during the CenBASE cruise, employing two commonly used techniques: eddy covariance and dual-tracer methods. The $K_{660}$ derived from both techniques agrees well, confirming the reliability of both methods for gas transfer velocity observations. The observed $CO_2$ transfer velocity shows a significant reduction compared to the open-ocean $CO_2$ observations and parameterisations under comparable wind conditions (Yang et al., 2024; Fig. 4). This reduction can be attributed to three competing processes (summarized in Fig. 8): 1) a 10% enhancement from fetch-limited increases in friction velocity, 2) an 18% suppression from reduced significant wave height, and 3) a 25% suppression from elevated surfactant concentrations. Together, these effects explain the overall 33% reduction in $CO_2$ exchange during CenBASE relative to the EC-based open ocean $K_{660\_CO2}$.

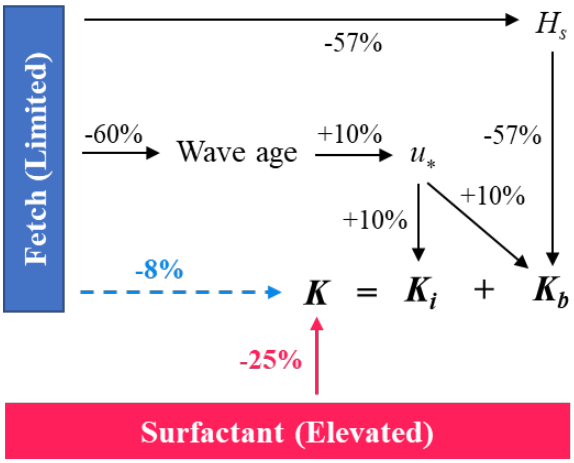


**Figure 8: Schematic illustrating how fetch and surfactants modulate the $CO_2$ transfer velocity (K) in the Baltic Sea relative to the open ocean.** Values denote the relative magnitude of enhancement (+) or suppression (–) for each process (Table 1). Black arrows and their associated values indicate the effect of fetch on individual gas exchange components, while the blue value on the dashed arrow shows the net fetch effect on total *K*. The red value and arrow represent the constrained surfactant-induced suppression of *K*.

During CenBASE, fetch lengths ranged from 50-300 km, in contrast to more than 1000 km in the open ocean. The limited fetch exerts both enhancing and suppressing effects on gas exchange in the Baltic Sea (Fig. 8). Shorter fetch produces a younger wave field dominated by shorter and

steeper waves, increasing surface roughness and thereby enhancing $u_*$ and $K_{660}$. At the same time, limited fetch constrains wave development, leading to a ~60% reduction in $H_s$ (Fig. 5A). As a key proxy for wave-breaking intensity (Brumer et al., 2017; Deike, 2021; Zhao et al., 2003), reduction in $H_s$ diminishes wave breaking and consequently suppresses bubble-mediated gas transfer (Dobashi & Ho, 2023; Fairall et al., 2006; Ocampo-Torres & Donelan, 1995; Woolf, 2005). These findings emphasize the need to incorporate sea-state dependence into $K_{660}$ parameterisations (Brumer, 2017; Deike & Melville, 2018; Fairall et al., 2022; Yang et al., 2024). When direct wave observations are unavailable, reanalysis products (e.g., ERA5; Hersbach et al., 2020) can serve as a first-order estimate of wave conditions for $K$ evaluation (Bessonova et al., 2025; Giudici et al., 2023).

Although bubble effects are expected to be stronger for low-solubility tracers such as $^3$He and $SF_6$ than for $CO_2$, the EC $CO_2$-derived and dual-tracer-derived $K_{660}$ values agreed closely (Fig. 4A). This is primarily because the bubble contribution to the total gas exchange during CenBASE was relatively small due to the low wind regime (Fig. 5B). According to the widely used model (Woolf, 1997), bubble-mediated transfer contributes ~25% to total $CO_2$ exchange and ~35% to $^3$He/$SF_6$ exchange under wind speeds of 0-12 m s$^{-1}$. This difference corresponds to only ~1.5 cm hr$^{-1}$ higher $K_{660}$ for dual tracers, which lies well within the measurement uncertainty and is therefore not practically distinguishable. Moreover, the much lower salinity in the Baltic Sea further limits the bubble-induced solubility dependence of $K$. Although the bubble size observations with the bubble cameras on a spar buoy did not work during CenBASE, it is well established that bubbles coalesce easily in fresh water (this is inhibited in salt water), so the initial bubble size distribution in fresher water quickly evolves towards larger bubbles through coalescence (e.g., De Leeuw et al., 2011). This coalescence effect has little influence on the gas transfer of moderately soluble gases such as $CO_2$ but reduces $K_b$ for very low-solubility gases (e.g., $^3$He and $SF_6$) due to the reduction of bubble surface area, thereby narrowing the difference in $K_{b660}$ between $CO_2$ and $^3$He/$SF_6$. This also indicates that the parameterisation of the bubble-mediated component derived from open-ocean EC data (Yang et al., 2024) remains applicable to the Baltic Sea, despite differences in salinity and, thereby, the bubble-size distribution.

The suppression of gas exchange by surfactants has been well documented in laboratory studies, which report 10-65% reductions in $K$ depending on surfactant concentration (Bock et al., 1999;

Frew et al., 1990; Goldman et al., 1988; Mesarchaki et al., 2015; Pereira et al., 2016; Pereira et al., 2018; Ribas-Ribas et al., 2018; Schmidt & Schneider, 2011). Based on the empirical relationship derived by Pereira et al. (2018) using laboratory data, the CenBASE microlayer surfactant concentration ($0.54 \pm 0.08$ mg $L^{-1}$) corresponds to an estimated ~20% reduction in $K$. Field studies have reported similar magnitudes of suppression (24-55%) under artificial surfactant additions (Brockmann et al., 1982; Salter et al., 2011). More recently, field chamber measurements indicate ~23% suppression for natural surfactant levels exceeding 0.2 mg $L^{-1}$ (Mustaffa et al., 2020), and EC-based $K_{660\_CO2}$ observations have shown ~30% suppression at moderate winds (~7 m $s^{-1}$) under likely high surfactant conditions (Yang et al., 2021). Thus, the 25% suppression estimated in this study agrees well with previous laboratory and field results.

Our findings refine the mechanistic understanding of air-sea gas exchange and have important implications for estimates of coastal $CO_2$ flux estimates. Using the $u_*$-$H_s$-$SA$ parameterisation, both summer uptake and winter outgassing of $CO_2$ in the Baltic Sea increase compared to a conventional $U_{10N}$-based parameterisation, amplifying the seasonal cycle. Because many coastal regions exhibit similarly short fetches and elevated surfactant concentrations (Fig. A6), the mechanism-based parameterisation proposed here is expected to yield systematically different gas exchange efficiencies than conventional wind-speed-based formulations. The mechanism-based $K$ parameterisation could alter coastal $CO_2$ flux estimates (e.g., Resplandy et al., 2024), influencing annual means, long-term trends, seasonal cycles, and spatial patterns. An improved estimate of the ocean $CO_2$ sink may also help reduce discrepancies between the data-based and model-based global carbon budgets (Friedlingstein et al., 2025). The improvement in the estimate of $K$ is especially important for mCDR studies, which are often tested or developed in coastal environments (e.g., Ho et al., 2024). Beyond $CO_2$, the updated parameterisation may also apply to other greenhouse gases, such as $N_2O$, which share the same interfacial exchange mechanism and exhibits similar bubble-mediated behavior due to their comparable solubility. Application to DMS is also possible, provided the bubble-mediated component is omitted.

Despite the advances from the CenBASE campaign, several uncertainties remain. The surfactant-induced suppression was inferred from residual differences between Baltic Sea and open-ocean $K_{660\_CO2}$ after correcting for fetch effects, and therefore carries considerable uncertainty even though the magnitude is consistent with previous field constraints. We were unable to partition the

surfactant-induced suppression between interfacial and bubble-mediated pathways because available evidence is insufficient to quantify their relative roles. Observations were limited to low-to-moderate wind speeds (<12 m $s^{-1}$), preventing evaluation of the surfactant effect under high wind-speed conditions. Furthermore, surfactant concentrations were relatively uniform during CenBASE, so suppression could not be assessed across natural SA concentration gradients. Given the strong seasonal and spatial variability in biological production, the transferability of our quantified suppression values beyond the CenBASE conditions is uncertain. Addressing these limitations will require coordinated, multi-season observations across diverse fetch conditions, surfactant regimes, and wind speeds. Such efforts are essential for building a generalizable framework for gas exchange in marginal seas and for improving both regional $CO_2$ budgets and assessment of emerging mCDR applications.

## Appendix

### A1. Dual-tracer experiments

The $K$ was also determined using the $^3He/SF_6$ dual tracer technique. $^3He$ and $SF_6$ were injected into the surface ocean, and their concentrations were monitored over time. Assuming that air-sea gas exchange is the only process affecting the $^3He/SF_6$ ratio, $K$ can be derived from the temporal change in their ratio. The two tracers, $^3He$ and $SF_6$, were injected with a molar ratio of 1:340 on 6 July 2022 at ~7 m depth for 40 minutes, centered at 57.263°N, 20.147°E. The injected tracers were then tracked using an underway $SF_6$ analysis system (Ho et al., 2002), which continuously measures the $SF_6$ concentration at the water surface, and the vessel-mounted acoustic Doppler current profiler (ADCP) (150 kHz Ocean Surveyor, RD Instruments).

Near the center of the patch of injected tracers, water samples were taken using the CTD rosette equipped with 13 5-L Niskin bottles. Discrete $SF_6$ samples were taken from the Niskin bottles using 250-ml syringes. The $SF_6$ concentration was measured onboard the ship using a gas chromatograph equipped with an electron capture detector (GC-ECD) in combination with a purge-and-trap system (Bullister and Weiss, 1988; Gerke et al., 2024). About 40 ml of seawater for discrete $^3He$ samples was collected in copper tubes placed in aluminum channels, with both ends sealed by stainless steel clamps. The $^3He$ samples were sent to the laboratory at the Institute of Environmental Physics at the University of Bremen after the cruise. There, $^3He$ was analyzed using a helium isotope mass spectrometer (MAP 215-50) (Sültenfuß et al., 2009).

### A2. Surfactant sampling

Surfactant samples from the SML were collected from a small workboat positioned ~500 m upwind of the research vessel. The SML was sampled using the glass-plate technique and transferred into amber borosilicate glass bottles (Cunliffe and Wurl, 2014; Harvey and Burzell, 1972). When weather conditions were unfavorable, SML sampling was conducted from the bow of the research vessel using a Garrett screen. For surfactant samples, 18 mL SML samples were transferred into acid-washed and pre-combusted (500 °C, 8 h) 20 mL glass vials and immediately frozen at −20 °C. Surface activity was analyzed within one year of collection by phase-sensitive alternating-current voltammetry using a 797 VA Computrace polarograph (Metrohm, Switzerland), following Cosović & Vojvodić (1982).

## A3. Wind speed distortion correction

During CenBASE, wind speed was measured using two instruments: a 2D sonic anemometer mounted on the ship's foremast (~17 m above MSL) and a 3D EC sonic anemometer on the front tower (~14 m above MSL) (Fig. 1). The foremast measurements are expected to be less distorted because of the higher position of the sensor (O'Sullivan et al., 2013) and are, therefore, used in this study. Nevertheless, previous work shows that the foremast-mounted anemometers can still be biased when the wind is not bow-on (e.g., Landwehr et al., 2018). To address this, we follow Landwehr et al. (2020) and use ERA5 reanalysis wind speeds, which are not affected by ship-relative flow distortions, to correct the ship measurements.

Because ERA5 winds may contain regional biases, we first calibrate ERA5 using in situ measurements from the Östergarnsholm station (Rutgersson et al., 2020). Winds from five measurement heights (normalized to $U_{10}$) are highly consistent, supporting the robustness of the station record (Fig. A8). We then compare station winds with ERA5 winds extracted at the station location for the period March-December 2024. To avoid land contamination, only winds from the open sector (80°-160°; Rutgersson et al., 2020) are used. ERA5 is slightly lower than the station wind below 6 m $s^{-1}$ but higher at stronger winds (Fig. A8). Two linear regressions are applied to ERA5, resulting in good agreement with the station winds (Fig. A8). Although the ERA5 wave data used in this study are simulated by a wave model forced with ERA5 winds, which may contain minor biases, these are not expected to substantially affect the simulated wave fields (Durrant et al., 2013).

The corrected ERA5 winds are then extracted at the CenBASE cruise location and time to serve as a reference for correcting ship wind distortions. The ratio of ship to corrected ERA5 wind speed as a function of relative wind direction shows the expected distortion pattern (Fig. A9; Moat et al., 2006; B. Moat & Yelland, 2015). We fit this ratio using three functions according to the relative wind direction: (1) quadratic for -30° to 45°, (2) linear for -90° to -30°, and (3) linear for 45° to 90° (Fig. A9). This fitted relationship is used to correct the ship's wind speed. After correction, the ratio of ship to ERA5 wind speeds aligns closely with unity (Fig. A9).

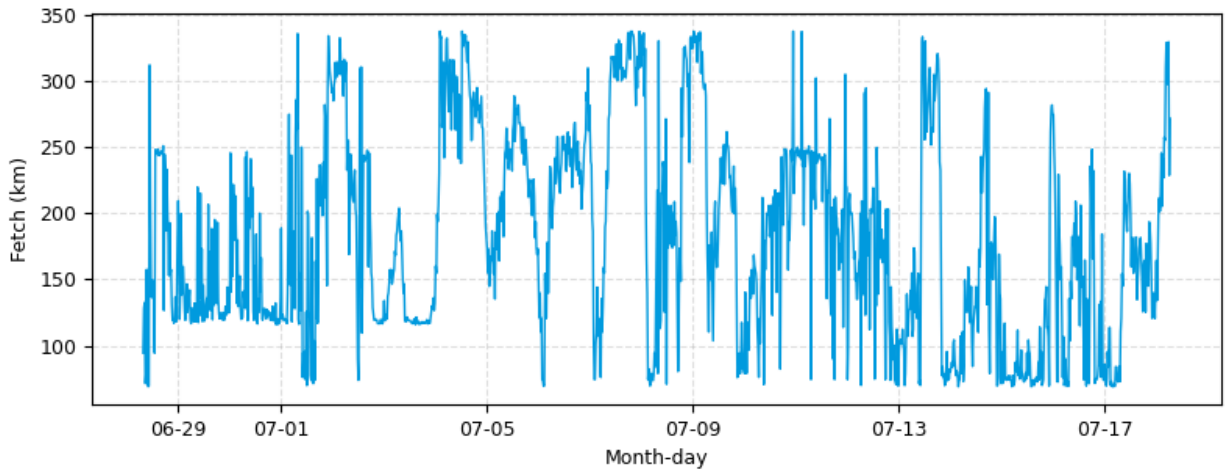


**Figure A1: Fetch of the location according to the CenBASE cruise track.** It is estimated based on the length to the land and the wind direction.

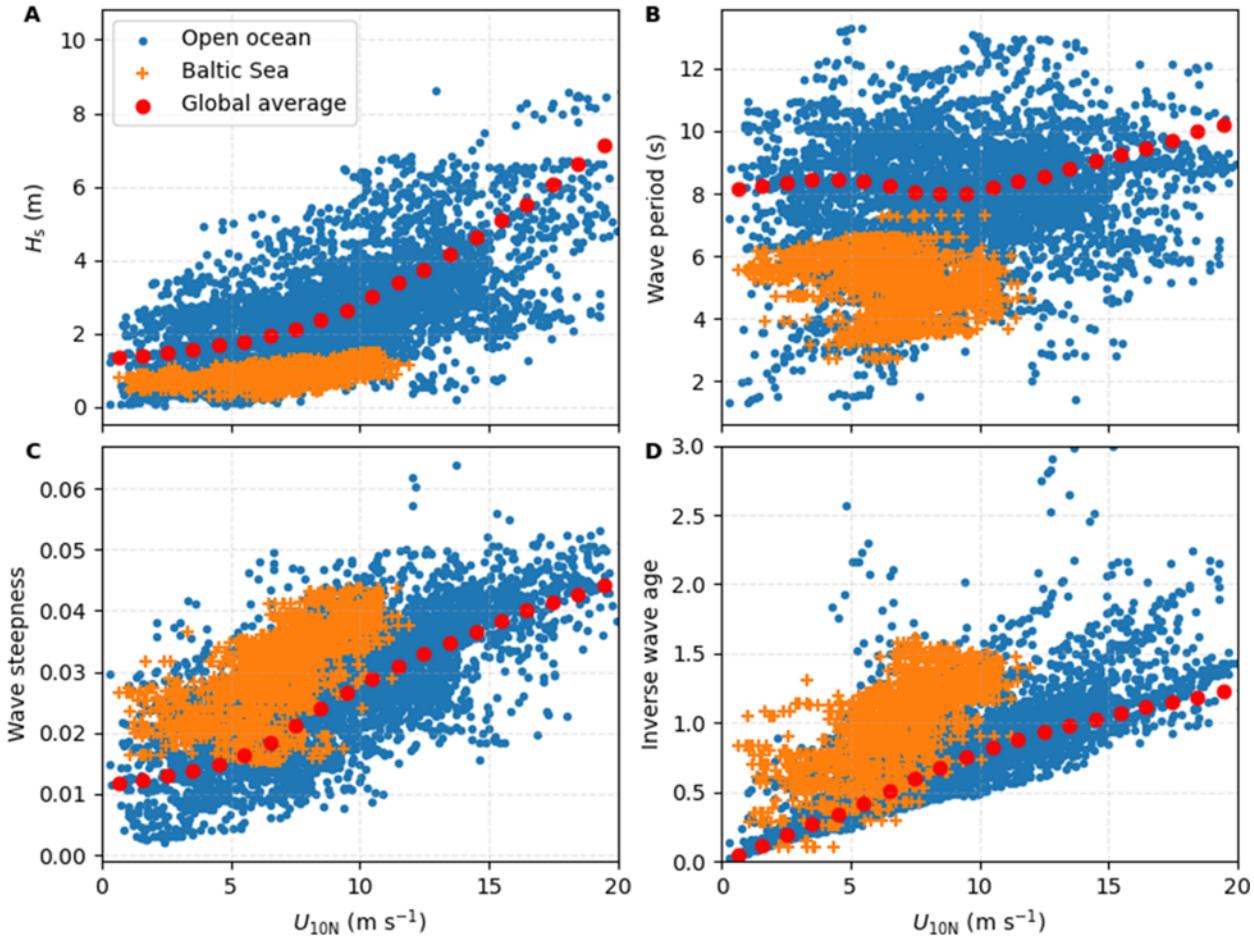


**Figure A2: Wave properties versus wind speed.** Orange: Waves in the Baltic Sea during CenBASE; Blue: Waves in open ocean cruises with eddy covariance measurements (see Yang et al., 2022); and Red: Waves in the global ocean average. For the global ocean average, we use the year 2024 as an example and take the first day of each month at 00:00 to capture seasonal variability. **A**: Significant wave height; **B**: Wave period; **C**: Wave steepness; **D**: Inverse wave age. See section 2.3 of the Method for information on wave data extraction.

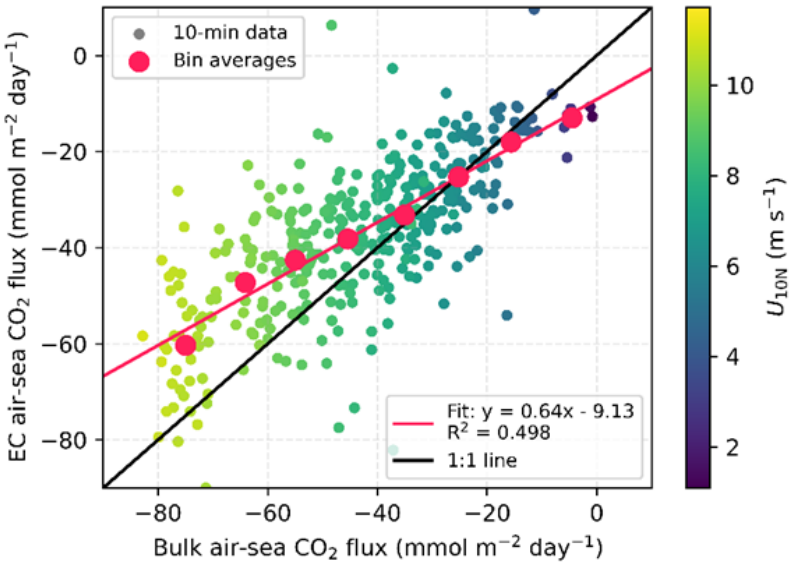


633

634 **Figure A3: Bulk air-sea $CO_2$ flux estimates versus EC air-sea $CO_2$ flux observations.** The Ho et al.
635 (2006) parameterisation is used for the bulk flux estimate. The small dots are 10-minute flux data, and the
636 large red dots represent the bin averages for every 10 mmol $m^{-2}$ $day^{-1}$ flux interval. The EC flux observations
637 are lower in magnitude than the bulk flux estimates at wind speeds higher than ~7 m $s^{-1}$.

638

639

640

641

642

643

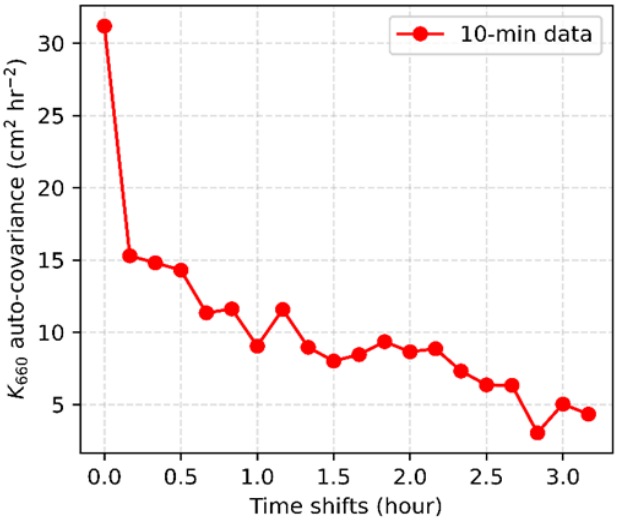


644

645 **Figure A4: Auto-covariance of EC-derived $CO_2$ transfer velocities ($K_{660}$).** The 10-min $K_{660}$ time series
646 from 4-7 July, selected for its continuity (see Fig. 1F), was used for this analysis. The first point represents
647 the variance of the $K_{660}$ time series, while the second point shows the covariance between the original series
648 and a version shifted by one point (i.e., 10-min). The decrease from the first to the second point indicates
649 the random uncertainty in this $K_{660}$ time series (~50%). This uncertainty can be further reduced to ~20% for
650 a 1-hour average (i.e., $50\%/\sqrt{6}$).

651

652

653

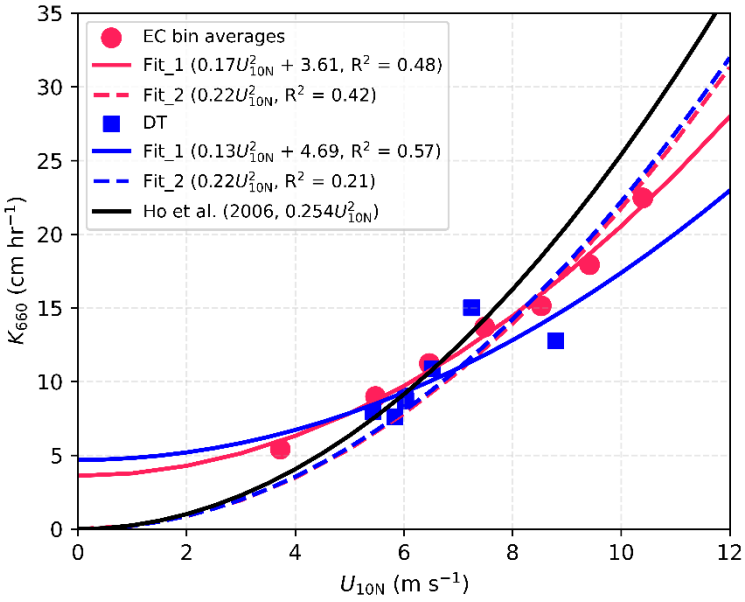


654

655 **Figure A5: Observed and parameterised gas transfer velocities ($K_{660}$).** Red dots show 10-min EC-
656 derived bin averages (for each 1 m s$^{-1}$ $U_{10N}$ bin), with red lines representing parameterisations fitted to these
657 data. Blue squares denote DT-derived $K_{660}$ values (timescale ~1 day), with blue lines showing
658 corresponding parameterisations. Solid lines follow the fitting form $K_{660} = aU_{10N}^2 + b$, while dashed lines
659 follow $K_{660} = aU_{10N}^2$.

660

661

662

663

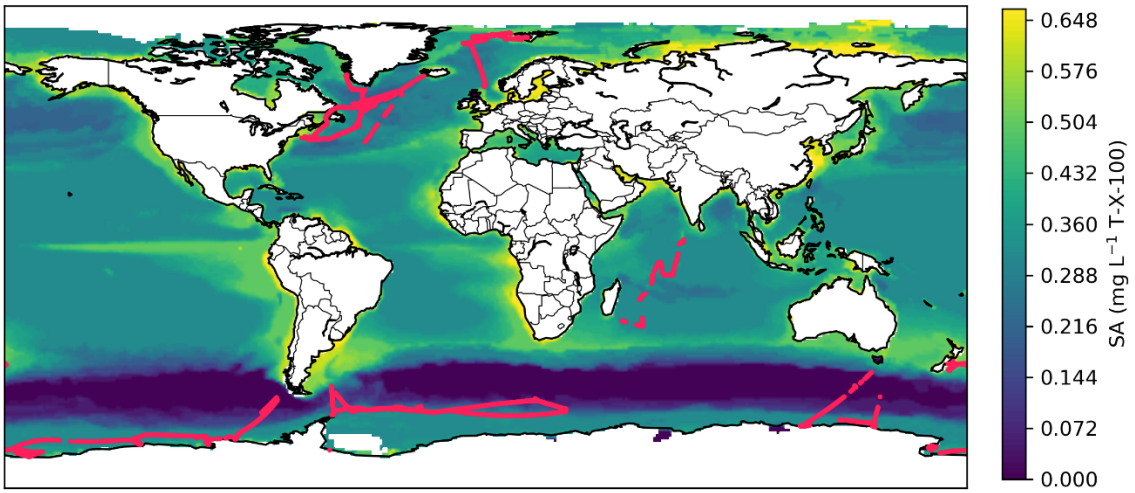


664

665 **Figure A6: Estimated surfactant distributions in the global ocean and the open ocean EC cruise**
666 **tracks.** The surfactant concentration is estimated following Wurl et al (2011) shown here as an annual mean.
667 Red lines indicate the EC cruises that were synthesized in Yang et al. (2022).

668

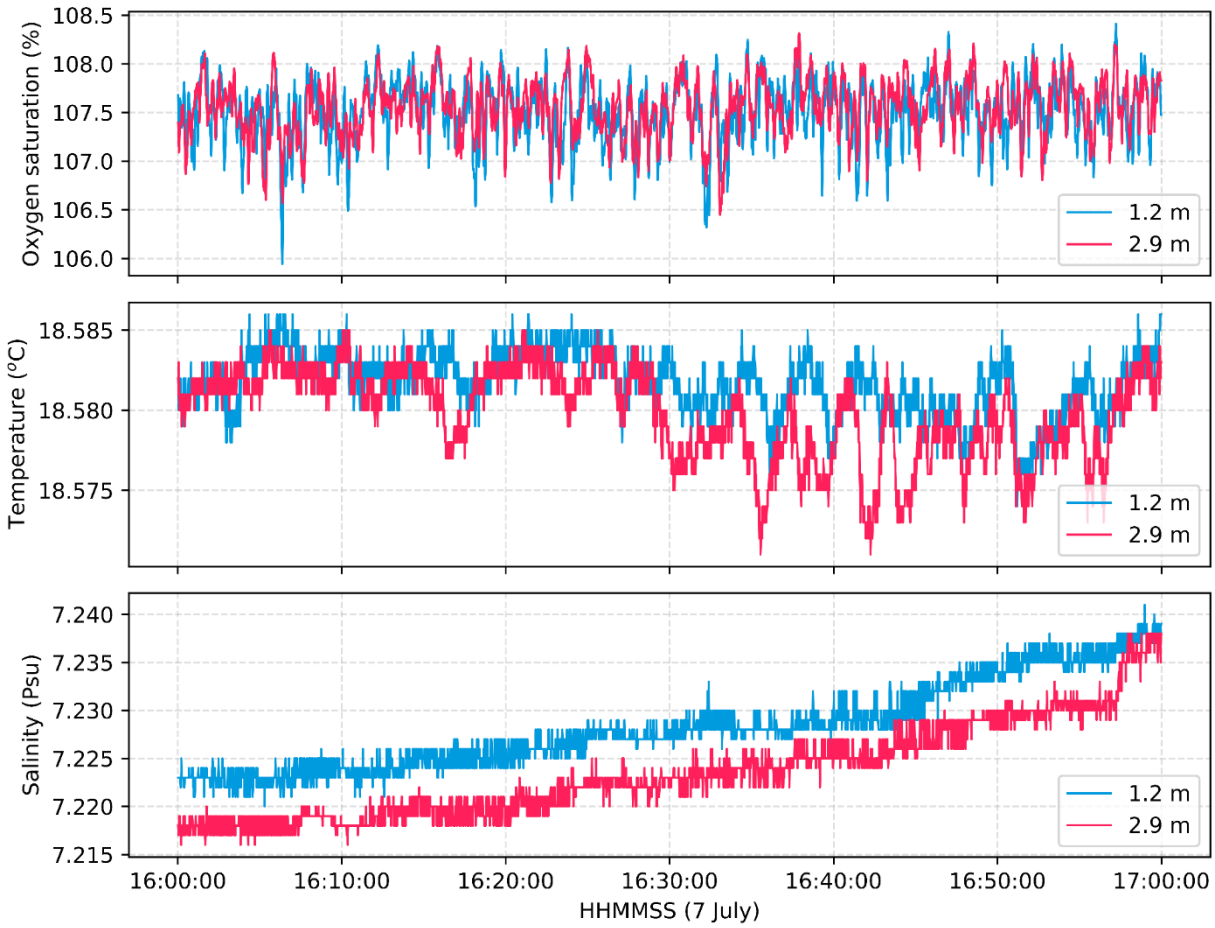


669

670 **Figure A7: Representative dissolved oxygen, salinity and temperature data from the small spar buoy,**
671 **showing the differences measured at 1.2m and 2.9m depth.** The patterns shown here are typical of both
672 day and night measurement periods.

673

674

675

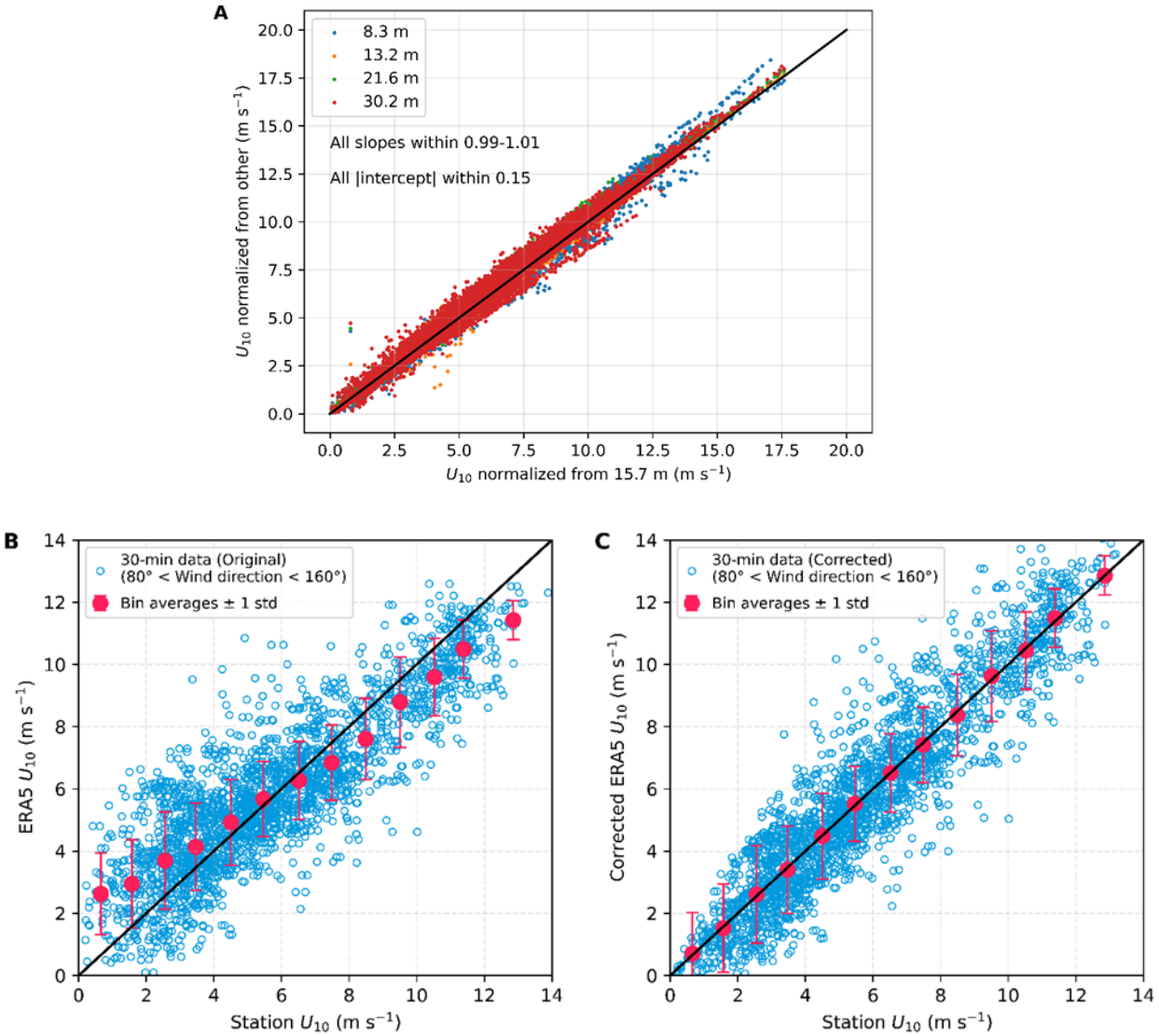


**Figure A8: Correction of ERA5 wind speed using reference measurements from the Östergarnsholm station (restricted to the open sector, 80°-160°; Rutgersson et al., 2020). A:** Comparison of the wind speed measurements from different heights at the Östergarnsholm station. All wind speeds were normalized to 10-meter height above MSL ($U_{10}$). **B:** Comparison of the station $U_{10}$ measurements and the extracted ERA5 $U_{10}$ at the location of the Östergarnsholm station. The red points are bin averages with error bars representing 1 standard deviation. The red points in panel B are fitted with two linear relationships: (1) $y = 0.64x + 2.05$ for station $U_{10} < 7.5$ m s$^{-1}$, and (2) $y = 0.88x + 0.28$ for station $U_{10} > 7.5$ m s$^{-1}$ for correction. **C:** Comparison of the station and ERA5 $U_{10}$ after the corrections using the relations in panel B.

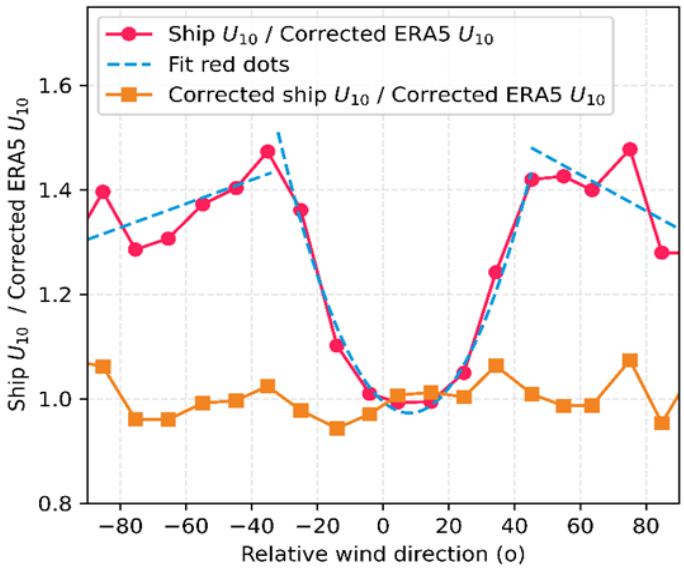


687

688 **Figure A9: Ratio of ship wind speed to subsampled ERA5 wind speed before (red) and after**
689 **correction (yellow) as a function of relative wind direction (RWD).** ERA5 wind speeds were first
690 calibrated against the Östergarnsholm station record (Fig. A8). The fitted relationships (blue) are: (1) $y$ =
691 0.00036(RWD - 8)$^2$ + 0.97 for -30° to 45°, (2) $y$ = 0.0023RWD + 1.51 for -90° to -30°, and (3) $y$ = -
692 0.0035RWD + 1.64 for 45° to 90°.

693

694

## Code and data availability

The code that was used to produce the figures is available in the supplementary material. The processed 10-min EC $CO_2$ fluxes, wind speeds, friction velocity, and gas transfer velocity can be found in the supplementary material.

## Supplement link

The link to the supplement will be included by Copernicus

## Author contributions

CM, DH, AE, and GR designed the project. YD processed and analyzed the data in consultation with CM, DH, and RD. CM collected the eddy covariance measurements; HCB collected the $CO_2$ fugacity data; and JK, AE, and BS collected the surfactant data. The dual-tracer data were provided by RD and DH. HC collected the spar buoy measurements. YD prepared the first draft of the manuscript, and all co-authors contributed to and approved the final version.

## Competing interests

The authors declare that they have no conflict of interest.

## Disclaimer

Copernicus Publications remains neutral with regard to jurisdictional claims made in the text, published maps, institutional affiliations, or any other geographical representation in this paper. While Copernicus Publications makes every effort to include appropriate place names, the final responsibility lies with the authors. Views expressed in the text are those of the authors and do not necessarily reflect the views of the publisher

## Acknowledgements

We thank the captains and crew of the *RV Elisabeth Mann Borgese*, T. Steffens (GEOMAR) for running the $CO_2$ flux system, and Matthis Björner and Michael Glockzin (IOW) for running/postprocessing the MESS data. We greatly appreciate F. Göhring (Deutscher Wetterdienst), Dr. M. Yang (Plymouth Marine Laboratory), Dr. J. Bidlot (European Centre for Medium-Range Weather Forecasts), Dr. A. Rutgersson (Uppsala University), Dr. J. Edson (Woods Hole Oceanographic Institution), and A. Körtzinger for helpful discussions. Data analysis and

visualization were completed using Python. ChatGPT was used to carefully polishing the manuscript's language to improve readability.

## Financial support

In this study, Y. Dong has been supported by the Alexander von Humboldt Foundation. R. Dobashi acknowledges the support from the Crown Prince Akihito Scholarship and the Uehiro Foundation on Ethics and Education. The ICOS station Östergarnsholm is funded by the Swedish Research Council and Uppsala University. Ship time was provided by the Leibniz Institute for Baltic Sea Research (IOW). The 3He/SF6 study was funded by the US National Science Foundation through OCE-2123997.

## Reference


Bell, T. G., Landwehr, S., Miller, S. D., De Bruyn, W. J., Callaghan, A. H., Scanlon, B., et al.: Estimation of bubble-mediated air-sea gas exchange from concurrent DMS and $CO_2$ transfer velocities at intermediate-high wind speeds, Atmos. Chem. Phys., 17, 9019–9033, https://doi.org/10.5194/acp-17-9019-2017, 2017.

Bessonova, V., Tapoglou, E., Dorrell, R., Dethlefs, N., & York, K.: Global evaluation of wave data reanalysis: Comparison of the ERA5 dataset to buoy observations, Appl. Ocean Res., 157, 104490, https://doi.org/10.1016/j.apor.2025.104490, 2025.

Bittig, H. C., Jacobs, E., Neumann, T., & Rehder, G.: A regional $pCO_2$ climatology of the Baltic Sea from in situ $pCO_2$ observations and a model-based extrapolation approach, Earth Syst. Sci. Data, 16, 753–773, https://doi.org/10.5194/essd-16-753-2024, 2024.

Blomquist, B. W., Brumer, S. E., Fairall, C. W., Huebert, B. J., Zappa, C. J., Brooks, I. M., et al.: Wind speed and sea state dependencies of air-sea gas transfer: Results from the High Wind Speed Gas Exchange Study (HiWinGS), J. Geophys. Res. Oceans, 122, 8034–8062, https://doi.org/10.1002/2017JC013181, 2017.

Blomquist, B. W., Huebert, B. J., Fairall, C. W., Bariteau, L., Edson, J. B., Hare, J. E., & McGillis, W. R.: Advances in air-sea $CO_2$ flux measurement by eddy correlation, Bound.-Lay. Meteorol., 152, 245–276, https://doi.org/10.1007/s10546-014-9926-2, 2014.

Bock, E. J., Hara, T., Frew, N. M., & McGillis, W. R.: Relationship between air-sea gas transfer and short wind waves, J. Geophys. Res. Oceans, 104, 25821–25831, https://doi.org/10.1029/1999JC900200, 1999.

Brockmann, U. H., Huhnerfuss, H., Kattner, G., Broecker, H., & Hentzschel, G.: Artificial surface films in the sea area near Sylt 1, Limnol. Oceanogr., 27, 1050–1058, https://doi.org/10.4319/lo.1982.27.6.1050, 1982.

Brumer, S. E., Zappa, C. J., Blomquist, B. W., Fairall, C. W., Cifuentes-Lorenzen, A., Edson, J. B., et al.: Wave-related Reynolds number parameterizations of $CO_2$ and DMS transfer velocities, Geophys. Res. Lett., 44, 9865–9875, https://doi.org/10.1002/2017GL074979, 2017.

759 Brumer, S. E., Zappa, C. J., Brooks, I. M., Tamura, H., Brown, S. M., Blomquist, B. W., et al.:
760 Whitecap coverage dependence on wind and wave statistics as observed during SO GasEx and
761 HiWinGS, J. Phys. Oceanogr., 47, 2211–2235, https://doi.org/10.1175/JPO-D-17-0005.1, 2017.

762 Bullister, J. L., & Weiss, R. F.: Determination of $CCl_3F$ and $CCl_2F_2$ in seawater and air, Deep-
763 Sea Res. Pt. A, 35, 839–853, https://doi.org/10.1016/0198-0149(88)90033-7, 1988.

764 Cole, J. J., & Caraco, N. F.: Atmospheric exchange of carbon dioxide in a low-wind oligotrophic
765 lake measured by the addition of SF6, Limnol. Oceanogr., 43, 647–656,
766 https://doi.org/10.4319/lo.1998.43.4.0647, 1998.

767 Cosović, B., & Vojvodić, V.: The application of ac polarography to the determination of surface-
768 active substances in seawater 1, Limnol. Oceanogr., 27, 361–369,
769 https://doi.org/10.4319/lo.1982.27.2.0361, 1982.

770 Cunliffe, M., & Wurl, O.: Guide to best practices to study the ocean's surface, Marine Biological
771 Association of the United Kingdom for SCOR, Plymouth, UK, http://plymsea.ac.uk/6523, 2014.

772 Deike, L.: Mass transfer at the ocean-atmosphere interface: The role of wave breaking, droplets,
773 and bubbles, Annu. Rev. Fluid Mech., 54, 191–224, https://doi.org/10.1146/annurev-fluid-
774 030121-014132, 2021.

775 Deike, L., & Melville, W. K.: Gas transfer by breaking waves, Geophys. Res. Lett., 45, 10482–
776 10492, https://doi.org/10.1029/2018GL078758, 2018.

777 Dobashi, R., & Ho, D. T.: Air-sea gas exchange in a seagrass ecosystem–results from a 3He/SF6
778 tracer release experiment, Biogeosciences, 20, 1075–1087, https://doi.org/10.5194/bg-20-1075-
779 2023, 2023.

780 Doney, S. C., Wolfe, W. H., McKee, D. C., & Fuhrman, J. G.: The science, engineering, and
781 validation of marine carbon dioxide removal and storage, Annu. Rev. Mar. Sci., 16, 1–27,
782 https://doi.org/10.1146/annurev-marine-040523-014702, 2024.

783 Dong, Y., Yang, M., Bakker, D. C. E., Kitidis, V., & Bell, T. G.: Uncertainties in eddy
784 covariance air-sea $CO_2$ flux measurements and implications for gas transfer velocity
785 parameterisations, Atmos. Chem. Phys., 21, 8089–8110, https://doi.org/10.5194/acp-21-8089-
786 2021, 2021.

787 Dong, Y., Jähne, B., Woolf, D. K., Krall, K. E., Yang, M., Czerski, H., et al.: The role of bubbles
788 in air-sea gas exchange: A critical review, Authorea [preprint],
789 https://doi.org/10.22541/essoar.175611263.31332921/v1, 2025.

790 Durrant, T. H., Greenslade, D. J. M., & Simmonds, I.: The effect of statistical wind corrections
791 on global wave forecasts, Ocean Model., 70, 116–131,
792 https://doi.org/10.1016/j.ocemod.2012.10.006, 2013.

793 Edson, J. B., Hinton, A. A., Prada, K. E., Hare, J. E., & Fairall, C. W.: Direct covariance flux
794 estimates from mobile platforms at sea, J. Atmos. Ocean. Technol., 15, 547–562,
795 https://doi.org/10.1175/1520-0426(1998)015<0547:DCFEFM>2.0.CO;2, 1998.

796 Edson, J. B., Jampana, V., Weller, R. A., Bigorre, S. P., Plueddemann, A. J., Fairall, C. W., et
797 al.: On the exchange of momentum over the open ocean, J. Phys. Oceanogr., 43, 1589–1610,
798 https://doi.org/10.1175/JPO-D-12-0173.1, 2013.

799 Fairall, C. W., Bariteau, L., Grachev, A. A., Hill, R. J., Wolfe, D. E., Brewer, W. A., et al.:
800 Turbulent bulk transfer coefficients and ozone deposition velocity in the International
801 Consortium for Atmospheric Research into Transport and Transformation, J. Geophys. Res.
802 Atmos., 111, 1–19, https://doi.org/10.1029/2006JD007597, 2006.

803 Fairall, C. W., Yang, M., Brumer, S. E., Blomquist, B. W., Edson, J. B., Zappa, C. J., et al.: Air-
804 sea trace gas fluxes: Direct and indirect measurements, Front. Mar. Sci., 9, 1–16,
805 https://doi.org/10.3389/fmars.2022.826606, 2022.

806 Frew, N. M.: The role of organic films in air-sea gas exchange, in: The Sea Surface and Global
807 Change, 121–172, https://doi.org/10.1017/CBO9780511525025.006, 1997.

808 Frew, N. M., Goldman, J. C., Dennett, M. R., & Johnson, A. S.: Impact of phytoplankton-
809 generated surfactants on air-sea gas exchange, J. Geophys. Res. Oceans, 95, 3337–3352,
810 https://doi.org/10.1029/JC095iC03p03337, 1990.

811 Frew, N. M., Bock, E. J., Schimpf, U., Hara, T., Haußecker, H., Edson, J. B., et al.: Air-sea gas
812 transfer: Its dependence on wind stress, small-scale roughness, and surface films, J. Geophys.
813 Res. Oceans, 109, 1–23, https://doi.org/10.1029/2003JC002131, 2004.

814 Friedlingstein, P., O'Sullivan, M., Jones, M. W., Andrew, R. M., Hauck, J., Landschützer, P., et
815 al.: Global Carbon Budget 2024, Earth Syst. Sci. Data, 17, 965–1039,
816 https://doi.org/10.5194/essd-17-965-2025, 2025.

817 Garbe, C. S., Rutgersson, A., Boutin, J., De Leeuw, G., Delille, B., Fairall, C. W., et al.: Transfer
818 across the air-sea interface, in: Ocean-atmosphere interactions of gases and particles, 55–112,
819 Springer, Berlin, Heidelberg, https://doi.org/10.1007/978-3-642-25643-1_2, 2014.

820 Gerke, L., Arck, Y., & Tanhua, T.: Temporal variability of ventilation in the Eurasian Arctic
821 Ocean, J. Geophys. Res. Oceans, 129, e2023JC020608, https://doi.org/10.1029/2023JC020608,
822 2024.

823 Giudici, A., Jankowski, M. Z., Männikus, R., Najafzadeh, F., Suursaar, Ü., & Soomere, T.: A
824 comparison of Baltic Sea wave properties simulated using two modelled wind data sets, Estuar.
825 Coast. Shelf Sci., 290, 108401, https://doi.org/10.1016/j.ecss.2023.108401, 2023.

826 Goldman, J. C., Dennett, M. R., & Frew, N. M.: Surfactant effects on air-sea gas exchange under
827 turbulent conditions, Deep-Sea Res. Pt. A, 35, 1953–1970, https://doi.org/10.1016/0198-
828 0149(88)90119-7, 1988.

829 Gutiérrez-Loza, L., Nilsson, E., Wallin, M. B., Sahlée, E., & Rutgersson, A.: On physical
830 mechanisms controlling air-sea $CO_2$ exchange, Biogeosciences, 19, 5645–5665,
831 https://doi.org/10.5194/bg-19-5645-2022, 2022.

832 Hammer, K., Schneider, B., Kuliński, K., & Schulz-Bull, D. E.: Acid-base properties of Baltic
833 Sea dissolved organic matter, J. Mar. Syst., 173, 114–121,
834 https://doi.org/10.1016/j.jmarsys.2017.04.007, 2017.

835 Harvey, G. W., & Burzell, L. A.: A simple microlayer method for small samples 1, Limnol.
836 Oceanogr., 17, 156–157, https://doi.org/10.4319/lo.1972.17.1.0156, 1972.

837 Ho, D. T., & Wanninkhof, R.: Air-sea gas exchange in the North Atlantic: $^3He/SF_6$ experiment
838 during GasEx-98, Tellus B, 68, 30198, https://doi.org/10.3402/tellusb.v68.30198, 2016.

839 Ho, D. T., Schlosser, P., & Caplow, T.: Determination of longitudinal dispersion coefficient and
840 net advection in the tidal Hudson River with a large-scale, high resolution $SF_6$ tracer release
841 experiment, Environ. Sci. Technol., 36, 3234–3241, https://doi.org/10.1021/es015814, 2002.

Ho, D. T., Law, C. S., Smith, M. J., Schlosser, P., Harvey, M., & Hill, P.: Measurements of air-sea gas exchange at high wind speeds in the Southern Ocean: Implications for global parameterizations, Geophys. Res. Lett., 33, L16611, https://doi.org/10.1029/2006GL026817, 2006.

Ho, D. T., Bopp, L., Palter, J., Long, M. C., Boyd, P., Neukermans, G., & Bach, L.: Monitoring, reporting, and verification for ocean alkalinity enhancement, in: Guide to Best Practices in Ocean Alkalinity Enhancement Research, 2-oae2023, 1–12, https://doi.org/10.5194/sp-2023-2, 2023.

Jähne, B. J., Münnich, K. O. M., Bösinger, R., Dutzi, A., Huber, W., & Libner, P.: On the parameters influencing air-water gas exchange, J. Geophys. Res., 92, 1937–1949, https://doi.org/10.1029/JC092iC02p01937, 1987.

Klavins, M., & Purmalis, O.: Humic substances as surfactants, Environ. Chem. Lett., 8, 349–354, https://doi.org/10.1007/s10311-009-0232-z, 2010.

Kunz, J., & Jähne, B.: Investigating small-scale air–sea exchange processes via thermography, Front. Mech. Eng., 4, 4, https://doi.org/10.3389/fmech.2018.00004, 2018.

Kuss, J., Nagel, K., & Schneider, B.: Evidence from the Baltic Sea for an enhanced $CO_2$ air-sea transfer velocity, Tellus B, 56, 175, https://doi.org/10.3402/tellusb.v56i2.16407, 2004.

Landwehr, S., Miller, S. D., Smith, M. J., Bell, T. G., Saltzman, E. S., & Ward, B.: Using eddy covariance to measure the dependence of air-sea $CO_2$ exchange rate on friction velocity, Atmos. Chem. Phys., 18, 4297–4315, https://doi.org/10.5194/acp-18-4297-2018, 2018.

Landwehr, S., Thurnherr, I., Cassar, N., Gysel-Beer, M., & Schmale, J.: Using global reanalysis data to quantify and correct airflow distortion bias in shipborne wind speed measurements, Atmos. Meas. Tech., 13, 3487–3506, https://doi.org/10.5194/amt-13-3487-2020, 2020.

De Leeuw, G., Andreas, E. L., Anguelova, M. D., Fairall, C. W., Lewis, E. R., O'Dowd, C., et al.: Production flux of sea spray aerosol, Rev. Geophys., 49, 1–39, https://doi.org/10.1029/2010RG000349, 2011.

McGillis, W. R., Edson, J. B., Ware, J. D., Dacey, J. W. H., Hare, J. E., Fairall, C. W., & Wanninkhof, R.: Carbon dioxide flux techniques performed during GasEx-98, Mar. Chem., 75, 267–280, https://doi.org/10.1016/S0304-4203(01)00042-1, 2001.

McGillis, W. R., Edson, J. B., Zappa, C. J., Ware, J. D., McKenna, S. P., Terray, E. A., et al.: Air-sea $CO_2$ exchange in the equatorial Pacific, J. Geophys. Res. Oceans, 109, C08S90, https://doi.org/10.1029/2003JC002256, 2004.

McKenna, S. P., & McGillis, W. R.: The role of free-surface turbulence and surfactants in air–water gas transfer, Int. J. Heat Mass Transfer, 47, 539–553, https://doi.org/10.1016/j.ijheatmasstransfer.2003.06.001, 2004.

Mesarchaki, E., Kräuter, C., Krall, K. E., Bopp, M., Helleis, F., Williams, J., & Jähne, B.: Measuring air-sea gas-exchange velocities in a large-scale annular wind-wave tank, Ocean Sci., 11, 121–138, https://doi.org/10.5194/os-11-121-2015, 2015.

Miller, S. D., Hristov, T. S., Edson, J. B., & Friehe, C. A.: Platform motion effects on measurements of turbulence and air-sea exchange over the open ocean. J. Atmos. Ocean. Technol., 25(9), 1683–1694, https://doi.org/10.1175/2008JTECHO547.1, 2008.

Miller, S. D., Marandino, C., & Saltzman, E. S.: Ship-based measurement of air-sea $CO_2$ exchange by eddy covariance, J. Geophys. Res. Atmos., 115, D02112, https://doi.org/10.1029/2009JD012193, 2010.

Moat, B., & Yelland, M.: Airflow distortion at instrument sites on the RRS James Clark Ross during the WAGES project, Natl. Oceanogr. Cent. Internal Doc., 12, http://nora.nerc.ac.uk/id/eprint/509304, 2015.

Moat, B. I., Yelland, M. J., & Cooper, E. B.: The airflow distortion at instruments sites on the RRS "James Cook", Natl. Oceanogr. Cent. Southampton Res. Consult. Rep., 11, 44 pp., http://eprints.soton.ac.uk/id/eprint/41147, 2006.

Mustaffa, N. I. H., Ribas-Ribas, M., Banko-Kubis, H. M., & Wurl, O.: Global reduction of in situ $CO_2$ transfer velocity by natural surfactants in the sea-surface microlayer, Proc. R. Soc. A, 476, 20190763, https://doi.org/10.1098/rspa.2019.0763, 2020.

Nightingale, P. D., Malin, G., Law, C. S., Watson, A. J., Liss, P. S., Liddicoat, M. I., et al.: In situ evaluation of air-sea gas exchange parameterizations using novel conservative and volatile tracers, Glob. Biogeochem. Cycles, 14, 373–387, https://doi.org/10.1029/1999GB900091, 2000.

O'Sullivan, N., Landwehr, S., & Ward, B.: Mapping flow distortion on oceanographic platforms using computational fluid dynamics, Ocean Sci., 9, 855–866, https://doi.org/10.5194/os-9-855-2013, 2013.

Ocampo-Torres, F. J., & Donelan, M. A.: On the influence of fetch and the wave field on the $CO_2$ transfer process: Laboratory measurements, in: Air–Water Gas Transfer, B. Jähne & E. C. Monahan (Eds.), AEON Verlag & Studio, Hanau, 543–552, 1995.

Parard, G., Charantonis, A. A., & Rutgersson, A.: Using satellite data to estimate partial pressure of $CO_2$ in the Baltic Sea, J. Geophys. Res. Biogeosci., 121, 1002–1015, https://doi.org/10.1002/2015JG003064, 2016.

Pereira, R., Schneider-Zapp, K., & Upstill-Goddard, R. C.: Surfactant control of gas transfer velocity along an offshore coastal transect: Results from a laboratory gas exchange tank, Biogeosciences, 13, 3981–3989, https://doi.org/10.5194/bg-13-3981-2016, 2016.

Pereira, R., Ashton, I., Sabbaghzadeh, B., Shutler, J. D., & Upstill-Goddard, R. C.: Reduced air-sea $CO_2$ exchange in the Atlantic Ocean due to biological surfactants, Nat. Geosci., 11, 492–496, https://doi.org/10.1038/s41561-018-0136-2, 2018.

Pitarch, J., Volpe, G., Colella, S., Krasemann, H., & Santoleri, R.: Remote sensing of chlorophyll in the Baltic Sea at basin scale from 1997 to 2012 using merged multi-sensor data, Ocean Sci., 12, 379–389, https://doi.org/10.5194/os-12-379-2016, 2016.

Prytherch, J., & Yelland, M. J.: Wind, convection and fetch dependence of gas transfer velocity in an Arctic sea-ice lead determined from eddy covariance $CO_2$ flux measurements, Glob. Biogeochem. Cycles, 35, e2020GB006633, https://doi.org/10.1029/2020GB006633, 2021.

Resplandy, L., Hogikyan, A., Müller, J. D., Najjar, R. G., Bange, H. W., Bianchi, D., et al.: A synthesis of global coastal ocean greenhouse gas fluxes, Glob. Biogeochem. Cycles, 38, 1–38, https://doi.org/10.1029/2023GB007803, 2024.

Ribas-Ribas, M., Helleis, F., Rahlff, J., & Wurl, O.: Air-sea $CO_2$ exchange in a large annular wind-wave tank and the effects of surfactants, Front. Mar. Sci., 5, 457, https://doi.org/10.3389/fmars.2018.00457, 2018.

Rutgersson, A., & Smedman, A.: Enhanced air-sea $CO_2$ transfer due to water-side convection, J. Mar. Syst., 80, 125–134, https://doi.org/10.1016/j.jmarsys.2009.11.004, 2010.

927 Rutgersson, A., Pettersson, H., Nilsson, E., Bergström, H., Wallin, M. B., Nilsson, E. D., et al.:
928 Using land-based stations for air-sea interaction studies, Tellus A, 72, 1–23,
929 https://doi.org/10.1080/16000870.2019.1697601, 2020.

930 Sabbaghzadeh, B., Upstill-Goddard, R. C., Beale, R., Pereira, R., & Nightingale, P. D.: The
931 Atlantic Ocean surface microlayer from 50°N to 50°S is ubiquitously enriched in surfactants at
932 wind speeds up to 13 m $s^{-1}$, Geophys. Res. Lett., 44, 2852–2858,
933 https://doi.org/10.1002/2017GL072988, 2017.

934 Sabbaghzadeh, B., Arévalo-Martínez, D. L., Glockzin, M., Otto, S., & Rehder, G.: Meridional
935 and cross-shelf variability of $N_2O$ and $CH_4$ in the eastern-south Atlantic, J. Geophys. Res.
936 Oceans, 126, e2020JC016878, https://doi.org/10.1029/2020JC016878, 2021.

937 Salter, M. E., Upstill-Goddard, R. C., Nightingale, P. D., Archer, S. D., Blomquist, B., Ho, D. T.,
938 et al.: Impact of an artificial surfactant release on air-sea gas fluxes during Deep Ocean Gas
939 Exchange Experiment II, J. Geophys. Res. Oceans, 116, C11007,
940 https://doi.org/10.1029/2011JC007023, 2011.

941 Schmidt, R., & Schneider, B.: The effect of surface films on the air-sea gas exchange in the
942 Baltic Sea, Mar. Chem., 126, 56–62, https://doi.org/10.1016/j.marchem.2011.03.007, 2011.

943 Sültenfuß, J., Roether, W., & Rhein, M.: The Bremen mass spectrometric facility for the
944 measurement of helium isotopes, neon, and tritium in water, Isot. Environ. Health Stud., 45, 83–
945 95, https://doi.org/10.1080/10256010902871929, 2009.

946 Upstill-Goddard, R. C.: Air-sea gas exchange in the coastal zone, Estuar. Coast. Shelf Sci., 70,
947 388–404, https://doi.org/10.1016/j.ecss.2006.05.043, 2006.

948 Vickers, D., & Mahrt, L.: Fetch limited drag coefficients, Bound.-Lay. Meteorol., 85, 53–79,
949 https://doi.org/10.1023/A:1000472623187, 1997.

950 Wanninkhof, R.: Relationship between wind speed and gas exchange over the ocean revisited,
951 Limnol. Oceanogr. Methods, 12, 351–362, https://doi.org/10.4319/lom.2014.12.351, 2014.

952 Wanninkhof, R., Asher, W. E., Ho, D. T., Sweeney, C., & McGillis, W. R.: Advances in
953 quantifying air-sea gas exchange and environmental forcing, Annu. Rev. Mar. Sci., 1, 213–244,
954 https://doi.org/10.1146/annurev.marine.010908.163742, 2009.

Weiss, R. F.: Carbon dioxide in water and seawater: the solubility of a non-ideal gas, Mar. Chem., 2, 203–215, https://doi.org/10.1016/0304-4203(74)90015-2, 1974.

Woolf, D. K., Land, P. E., Shutler, J. D., Goddijn-Murphy, L. M., & Donlon, C. J.: On the calculation of air-sea fluxes of $CO_2$ in the presence of temperature and salinity gradients, J. Geophys. Res. Oceans, 121, 1229–1248, https://doi.org/10.1002/2015JC011427, 2016.

Woolf, D. K.: Bubbles and the air-sea transfer velocity of gases, Atmos.-Ocean, 31, 517–540, https://doi.org/10.1080/07055900.1993.9649484, 1993.

Woolf, D. K.: Parametrization of gas transfer velocities and sea-state-dependent wave breaking, Tellus B, 57, 87, https://doi.org/10.3402/tellusb.v57i2.16783, 2005.

Woolf, D. K.: Bubbles and their role in gas exchange, in: The Sea Surface and Global Change, 173–206, Cambridge University Press, https://doi.org/10.1017/CBO9780511525025.007, 1997.

Wurl, O., Wurl, E., Miller, L., Johnson, K., & Vagle, S.: Formation and global distribution of sea-surface microlayers, Biogeosciences, 8, 121–135, https://doi.org/10.5194/bg-8-121-2011, 2011.

Yang, M., Smyth, T. J., Kitidis, V., Brown, I. J., Wohl, C., Yelland, M. J., & Bell, T. G.: Natural variability in air-sea gas transfer efficiency of $CO_2$, Sci. Rep., 11, 1–9, https://doi.org/10.1038/s41598-021-92947-w, 2021.

Yang, M., Bell, T. G., Bidlot, J. R., Blomquist, B. W., Butterworth, B. J., Dong, Y., et al.: Global synthesis of air-Sea $CO_2$ transfer velocity estimates from ship-based eddy covariance measurements, Front. Mar. Sci., 9, 1–15, https://doi.org/10.3389/fmars.2022.826421, 2022.

Yang, M., Moffat, D., Dong, Y., & Bidlot, J.-R.: Deciphering the variability in air-sea gas transfer due to sea state and wind history, PNAS Nexus, pgae389, https://doi.org/10.1093/pnasnexus/pgae389, 2024.

Zhao, D., Toba, Y., Suzuki, Y., & Komori, S.: Effect of wind waves on air-sea gas exchange: Proposal of an overall $CO_2$ transfer velocity formula as a function of breaking-wave parameter, Tellus B, 55, 478–487, https://doi.org/10.3402/tellusb.v55i2.16747, 2003.